Testing the suitability of luminescence dating on Quaternary badland deposits, Kula, Turkey

Coen de Jong

July, 2019

WAGENINGEN
UNIVERSITY & RESEARCH

Author: Coen de Jong
Registration number: 960202401080

Master thesis
Earth and Environment: Soil Geography and Earth Surface Dynamics

July, 2019
Wageningen, The Netherlands

Supervisors :

MSc S. Aksay
dr. T. Reimann
dr. J.M. Schoorl

Acknowledgements

First of all, I would like to thank my supervisors for all the advice, support and feedback they have given. I want to thank Selçuk Aksay for his help during the fieldwork and informing me about the study area. Furthermore, I would like to thank Alice Versendaal and Erna Voskuilen of the NCL-laboratory and Tony Reimann for the preparation, measurement and interpretation of the OSL data and for allowing me to use their equipment.

Abstract

Badlands are highly eroded and dynamic regions, which makes them geomorphologically very interesting. Yet, the formation, development and surface dynamics of these regions is often poorly understood. Through an in-depth description of the stratigraphy and OSL dating, the development of the Kula Badlands in western Turkey has been investigated. In this setting, OSL performance was expected to be poor due to lack of ample sunlight exposure and sufficient sensitive grains. With knowledge on recent advancements in luminescence dating over the past decades this study examines the suitability of OSL for the Kula badland deposits. Two different Luminescence dating techniques were used, namely the single aliquot regenerative (SAR) method for quartz and the post-IR IR SAR protocol for feldspar minerals. Optimal performance was achieved by tailoring the methods through the use of several performance tests. Results showed no clear influence of anomalous fading for pIRIR ages and by applying a Minimum Age Model to the equivalent dose distributions, it was possible to extract the well-bleached fraction and obtain reasonable age estimations for both quartz and feldspar. The quartz and feldspar ages are largely in agreement within the 2σ uncertainty, with a slight overestimation of the quartz ages. The poor efficiency and averaging of the quartz signal led to the conclusion that more reliable estimations can be achieved with feldspar grains. The stratigraphic reconstruction showed two disconnected successions of deposition, for which it was possible to assign an age of 0.7 ka and 1.3 ka, respectively. These young, late Holocene sediments illustrate the very recent and rapid development of the badlands.

Table of Contents

1. Introduction

The arid to semi-arid climate of the Mediterranean is ideal for the formation of badlands. Vegetation in these badlands is typically scarce and in combination with unconsolidated sediments and seasonally intense precipitation events, extensive erosion can shape the landscape. Erosion rates in these badlands are some of the highest in the world, yet very variable (Nadal-Romero et al., 2011). This makes them geomorphically very interesting, as can be seen from the numerous studies performed in these areas (Cerdà, 1999; Faulkner et al., 2000; Kuhn et al., 2004; Clarke and Rendell, 2006; García-Ruiz et al., 2013). The Kula Badlands are no different in this regard.

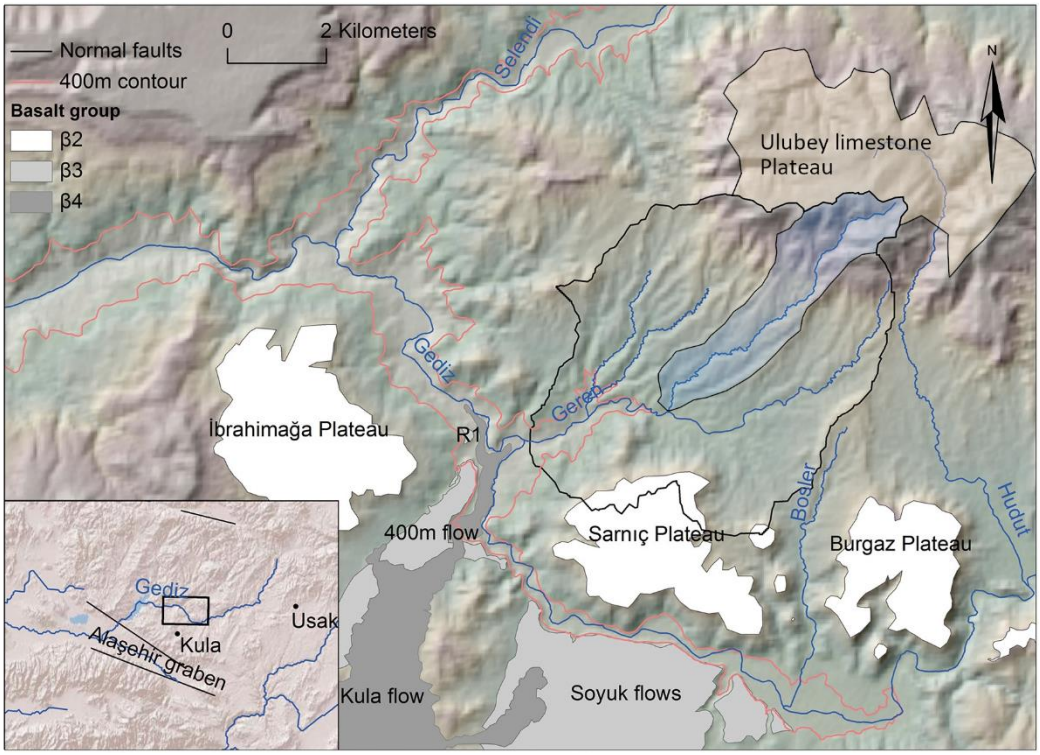

Figure 1 Location of the area of interest with the thick black lines indicating the Geren catchment which makes up most of the Kula Badlands. The blue shaded area is the sub-catchment which is of interest for this study (Redrawn from Van Gorp et al., 2016).

The Kula Badlands are located to the north of the Kula volcanic region, West Turkey. The badlands are characterised by deeply incised valleys adjacent to roughly SW-NE extended plateaux. The valleys are formed due to the incision by (tributaries of) the Gediz and Selendi rivers (Figure 1). This includes the Gediz, Geren, Hudut, Bozlar and Selendi catchments, though the focus in this study will be on (a sub-catchment of) the Geren catchment (Figure 1). The badland plateaux accommodate agricultural fields while the valleys are reserved for the natural vegetation due to steep slopes. Natural vegetation is predominantly Macchia of Quercus and Pinus and grass. This vegetation is typical for the Mediterranean climate that is found here with dry summers and wet winters and springs (Köppen-Geiger classification Csa; Beck et al., 2018). The area is bounded by a Miocene limestone plateau to the north and basalt plateaux of Mid-Quaternary volcanics to the south (Figure 1). Furthermore, signs of early habitation can be found in the region, which dates back as early as the Neolithic (Maddy et al., 2015). Traces of Hittite, ancient Greek, Roman and Byzantine settlements can still be found in the landscape in the form of pottery pieces and remnants of buildings. It is suggested for other badlands that they have been formed by a combination of

climatic and human influences (Casana, 2008; Clarke and Rendell, 2010), which might also be the case for the Kula Badlands. However, the actual formation and the causes for the initiation of the badlands remains poorly understood. The question of whether the recent tectonic activity, climate change and/or human activity have played a role in the development of the Kula Badlands is still under investigation (Aksay, 2018). Also, despite various studies having investigated the pre-Quaternary deposits in the region, the Quaternary sediments have received little attention. The problem is the lack of comprehensive stratigraphic data and absolute dating techniques for Quaternary deposits. Examining the stratigraphy of badlands sediments with age control provides a better understanding on the formation, causes and development rates of badlands.

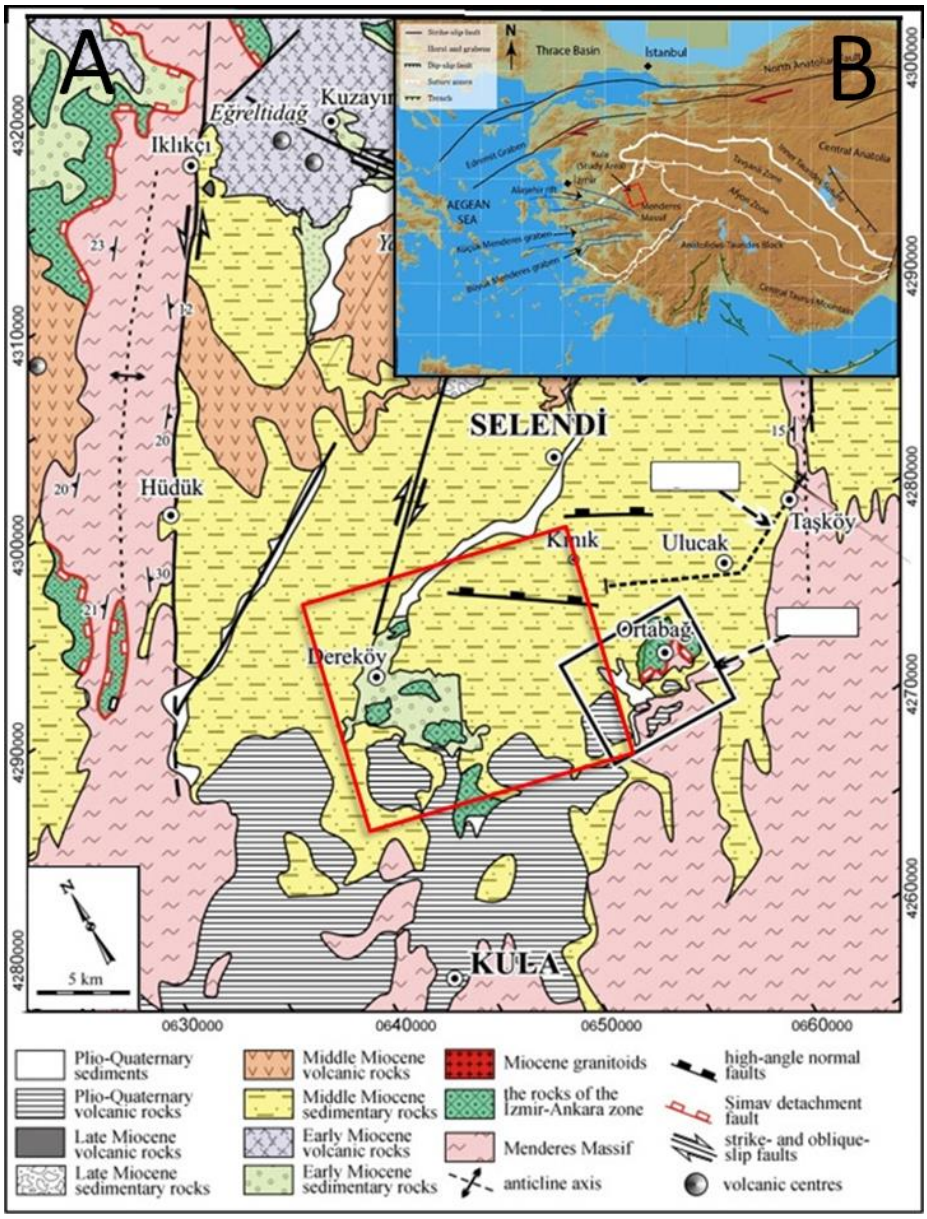

Figure 2 (A) Geology of the Kula Badlands (red square) and the surrounding area (Redrawn from (Ersoy et al., 2010)) and (B) the location of this area (red rectangle) in western Turkey with major tectonics (Aksay, 2018).

The Kula Badlands are located in the so-called Selendi Basin (Figure 2; Seyitoğlu, 1997). This basin formed during the late Cenozoic as a result of crustal extension (Ersoy et al., 2010). The Basin infill started during the Miocene, unconformably covering the metamorphic basement. These infill sediments, namely the Inay group, can be subdivided into the Ahmetler formation and Ulubey formation as lower and upper layer, respectively (Figure 3). The Ahmetler formation consists of basal conglomerates and fluvial sandstones and siltstones, while the Ulusbey formation is made up of horizontal, mostly carbonate sediments of lacustrine origin (Ersoy et al., 2008, 2010). In the Kula Badlands the Ulubey Formation is almost completely removed except for the plateau in the north (Figure 1), which is mostly preserved due to the resistant carbonates (Maddy et al., 2008). It is mainly the Ahmetler Formation that is currently being incised by the various rivers. However, there are still Quaternary sediments to be found in this area, which are sediments eroded from Ahmetler and Ulubey Formations. These sediments are the focus of this research. To the south, plateaux of lava flows from early Pleistocene volcanic events can be found (Richardson-Bunbury, 1996). These lava flows are part of several phases of volcanism of which the youngest happened ~3000 years ago. This youngest lava flow can be found downstream at the Geren/Gediz confluence, which has caused the damming of the contemporary Gediz and Geren rivers (Van Gorp et al., 2013, 2014, 2016). The reader is referred to previous publications for further details on the geology and stratigraphy of Kula and its surroundings (Seyitoğlu, 1997; Purvis and Robertson, 2004; Ersoy et al., 2008, 2010; Veldkamp et al., 2015).

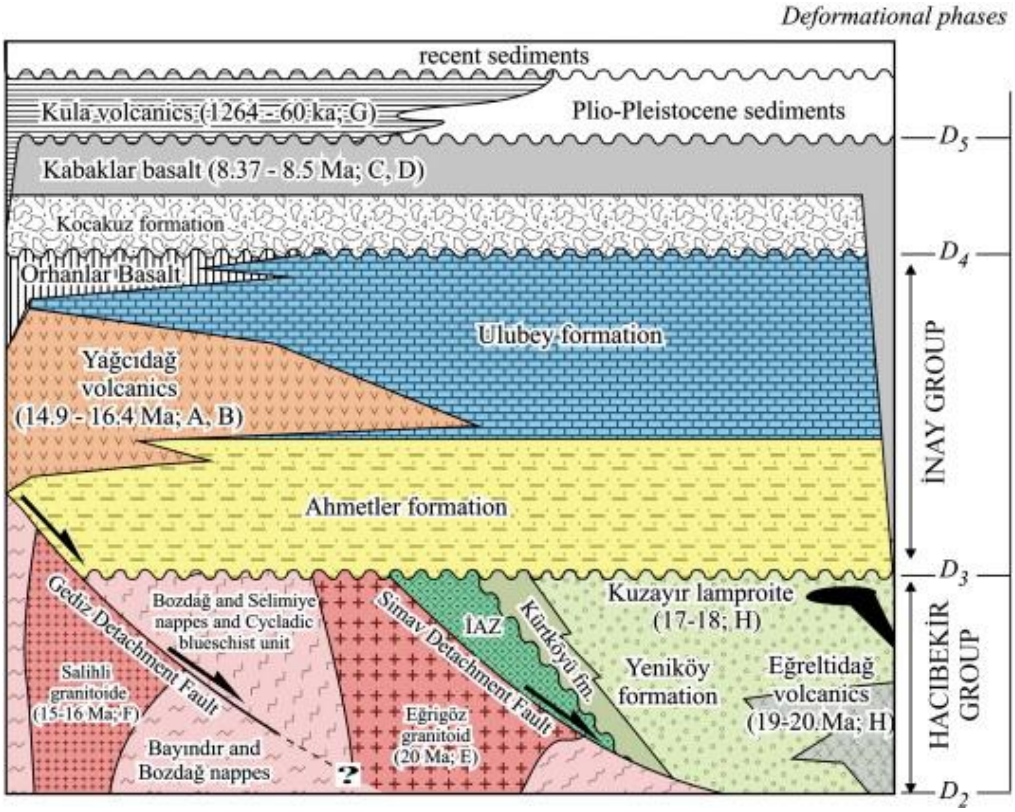

Figure 3 Tectono-stratigraphic units of the Selendi basin (from Ersoy et al., 2010).

For absolute age dating of the Quaternary sediments, Optically Stimulated luminescence (OSL) will be used. However, to fully understand the context of the ages and to make sure the most useful samples are collected, it is essential to understand the stratigraphy from which the samples are collected. Furthermore,

the suitability of OSL is dependent on the type of sediments and depositional environment, which is usually site specific (Preusser et al., 2006; Steffen et al., 2009; Reimann et al., 2011). Due to the large difference in precipitation during the year, combined with easy to erode bedrock and sediments, the sediment transport in the Kula Badlands is highly dynamic. Also, the Geren catchment is relatively small and because of this the sediment transport distance is also small. This may lead to synchronous erosion and deposition, which increases the complexity of the landscape dynamics even further. The high variability in sediment discharge translates to variation in the suitability of the sedimentary units for OSL. For this reason, an in-depth description of the stratigraphy of the Quaternary sediments in this setting is needed to get a grasp of the different sedimentary units that are present in these badlands. However, due to the extensive erosion, the terrain is difficult to traverse and outcrops may not be accessible at locations. Nevertheless, several sedimentary successions have been described and correlated.

For absolute age dating of Quaternary sedimentary units, luminescence dating, in particular OSL, has become one of the most sound methodologies during the past decade considering the recent advancements in the technique (Rhodes, 2011). However, this technique comes with a lot of uncertainties (See chapter 2). As mentioned before the incising trunk streams and gullies of the badlands are only several km long and because of this the distance that sediments may travel is very limited. This results in limited exposure to daylight and therefore it decreases the chance of proper bleaching (Chapter 2). For both quartz and feldspar this poor bleaching is an important factor, but in particular the feldspar minerals are affected by this, since the feldspar signal takes considerably longer to bleach than the quartz signal (Godfrey-Smith et al., 1988; Thomsen et al., 2008). Poor or insufficient bleaching is therefore a larger risk when working with feldspar possibly leading to an overestimation of the age. On the other hand, feldspar usually provides brighter luminescence signals, thus making it more likely to measure a detectable signal. The small size of the catchment also means that the amount of times a grain can be eroded and deposited since erosion from the pre-Quaternary sediments/bedrock is likely limited, which influences the sensitivity of the minerals. With multiple cycles of light exposure and burial since erosion from the bedrock, quartz grains tend to become more sensitive (Pietsch et al., 2008). Since the distances from bedrock are short, it is unlikely that a lot of burial cycles occurred, thus resulting in signals that might be too low for accurate dating. Also, the percentage of quartz grains that provide a detectable luminescence signal is considerably lower than for feldspar (Duller et al., 2003). Nevertheless, in highly dynamic geomorphic settings quartz OSL is preferred because of its fast bleaching properties and its stable luminescence signal (Wintle et al., 1995; Kars et al., 2014). To investigate whether this is reasonable, both quartz and feldspar procedures will be used for age estimations since feldspar can circumvent most of the problems related to quartz (Chapter 2).

In this study I examine the evolution of the Kula badlands within a sub-catchment of the Geren catchment by combining the stratigraphy and numerical ages obtained from OSL. The suitability of the OSL technique to accurately estimate the ages of the Quaternary sediments in the Kula Badlands is also investigated. This will be achieved by; (1) executing a series of performance tests to tailor a quartz and feldspar protocol, (2) Cross-validating the quartz and feldspar protocols and their resulting ages and (3) correlating the numerical ages with the stratigraphy. The produced data is used to construct a geochronology and discuss the development of the badlands.

2. Introduction to OSL

The dating of the Quaternary deposits will be done using Optically Stimulated Luminescence (OSL) dating technique. This method uses luminescence signals that are produced when quartz and feldspar grains are stimulated with light to infer the age of the sediments (Rhodes, 2011). When sand grains are buried, electrons are exposed to ionizing radiation from the surrounding sediments which causes electrons to get trapped in defects of the mineral structure of the grains. Over time the trapped charge accumulates at a rate proportional to the time since burial. If the grains become exposed to light, or high temperatures, the electrons recombine. During recombination, light is emitted which can be measured in the laboratory. After recombination, the luminescence signal is reset, which is called bleaching (Godfrey-Smith et al., 1988; Wallinga, 2008). Generally, an older sediment will produce a stronger luminescence signal (Rhodes, 2011). In the laboratory a dose response curve is constructed, which is the increase in luminescence signal related to the increase in applied dose. The dose response curve is the increase in luminescence signal related to increase in applied dose. The dose corresponding to the natural luminescence signal of the grains can be estimated from this curve and is called the equivalent dose (D_e) (Wallinga et al., 2000). By applying several rejection criteria it is possible to isolate grains which provide a useful equivalent dose. From the distribution of these remaining doses the best bleached population can be identified by applying an appropriate model depending on the type of distribution (Reimann et al., 2012b). The resulting value representing this best bleached population is referred to as the burial dose.

In addition to the burial dose, the dose rate is required for the age determination, which is the annual ionizing radiation dose received from the surrounding materials (Rhodes, 2011). It is an estimate based on the measurement of radionuclide concentrations in the sample with the use of gamma spectrometry (Wallinga et al., 2007). The geographical, lithological and hydrological context must be considered in order to estimate the amount of cosmic radiation and the effects of attenuation by the water content and organic matter. Additionally for feldspar, the internal dose rate from ^{40}K has to be taken into consideration. The dose rate is calculated in gray per thousand years (Gy/ka). The age can now be calculated as the burial dose divided by the dose rate. A more elaborate review of OSL techniques can be found in Rhodes (2011).

When working with OSL two types of minerals are usually used, quartz and (K-)feldspar. Typically, quartz is used for two reasons. First, quartz provides a stable OSL signal (Kars et al., 2014). Secondly, quartz has a short bleaching time, which means that there is less chance of inherited luminescence signals that could lead to an age overestimation (Wintle et al., 1995; Clarke, 1996). The use of feldspar is another option. For feldspar the infrared signal is usually measured using Infra-Red Stimulated Luminescence (IRSL) (Wintle et al., 1995). The advantage is that feldspar has a much brighter luminescence signal compared to quartz (Godfrey-Smith et al., 1988; Lukas et al., 2007). This means that in cases where quartz signals are almost undetectable, feldspar with its brighter luminescence signal may provide a better chance for dating the sediments. On the other hand, using feldspar comes with two disadvantages; slower bleaching of the IRSL signal and anomalous fading (Wallinga et al., 2007; Thomsen et al., 2008). Anomalous fading leads to an underestimation of the age due to a loss of the signal (Kars et al., 2014). However, it is possible to minimise the anomalous fading by applying a post-InfraRed IRSL (pIRIR) protocol (Thomsen et al., 2008). With this method an IRSL signal is measured at an elevated temperature after a standard IRSL signal at 50 °C is measured. Higher temperatures should result in more stable signals (Jain and Ankjærgaard, 2011; Smedley et al., 2015). However, it also means that the resulting signal takes more time to bleach (Kars et al., 2014). To account for the slower bleaching rates of feldspar, a single-grain analysis (Duller et al., 2003) can be performed to differentiate the well bleached grains from the poorly bleached grains.

3. Experimental details

3.1. Stratigraphy

To fully understand the extent of the Quaternary sediments and the development of the badlands, a fieldtrip was undertaken during the spring of 2019. This was a continuation of previous fieldtrips by the leading members of the "Temperate Mediterranean Badlands: A (pre-)Holocene or Anthropocene phenomenon?" project (Aksay, 2018). During these field campaigns various outcrops within the study area were observed, described and mapped to find suitable sampling locations for OSL and to understand the sedimentary succession. With the profile descriptions attention is paid to the lithology, topography, orientation, flow direction and grain-size of sediments and according to these criteria sedimentary units were distinguished. A compass was used for determining the orientation of outcrops and faults, if present. The position and elevation of the outcrops were determined using a handheld "Garmin ETrex 20x" GPS. The thicknesses of the outcrops and the sedimentary units were determined with a measuring tape at locations which were easily accessible. In other situations, it is either a visual estimation or based on photographs (with objects of known size for comparison). The lithology is determined by a visual inspection of the grains and clasts.

3.2. Sample preparation

3.2.1. Sampling

In this study a particular focus will be on one of the sub-catchments of the Geren river (Figure 1). For this sub-catchment, a total of five samples were used which were collected from three locations (named KG07, KG08 and KG09; Table 1; Figure 4). The five samples will be referred to as NCL-1218128 - 1218132, assigned by the NCL laboratory. The samples were collected at strategically chosen locations from easily accessible outcrops on an earlier fieldtrip by the project team. The (parts of) sedimentary units containing mostly coarse material like pebbles were avoided for sampling. The procedure includes hammering plastic tubes into the outcrop and sealing them with aluminium foil and black tape, that is to prevent a possible contamination through daylight exposure. Careful attention was given to keep the exposure to a minimum when removing each tube from the outcrop. Also, the outer parts of the sample in the tube were removed to exclude grains which might have been exposed to daylight during sampling.

Table 1 UTM coordinates of the outcrops were OSL samples were taken, with the bottom elevation in meters above mean sea level.

Location Code	**X-coordinate (UTM)**	**Y-coordinate (UTM)**	**Elevation (m a.m.s.l.)**
KG07	0654883	4280824	498
KG08	0655174	4281105	502
KG09	0655015	4280973	503

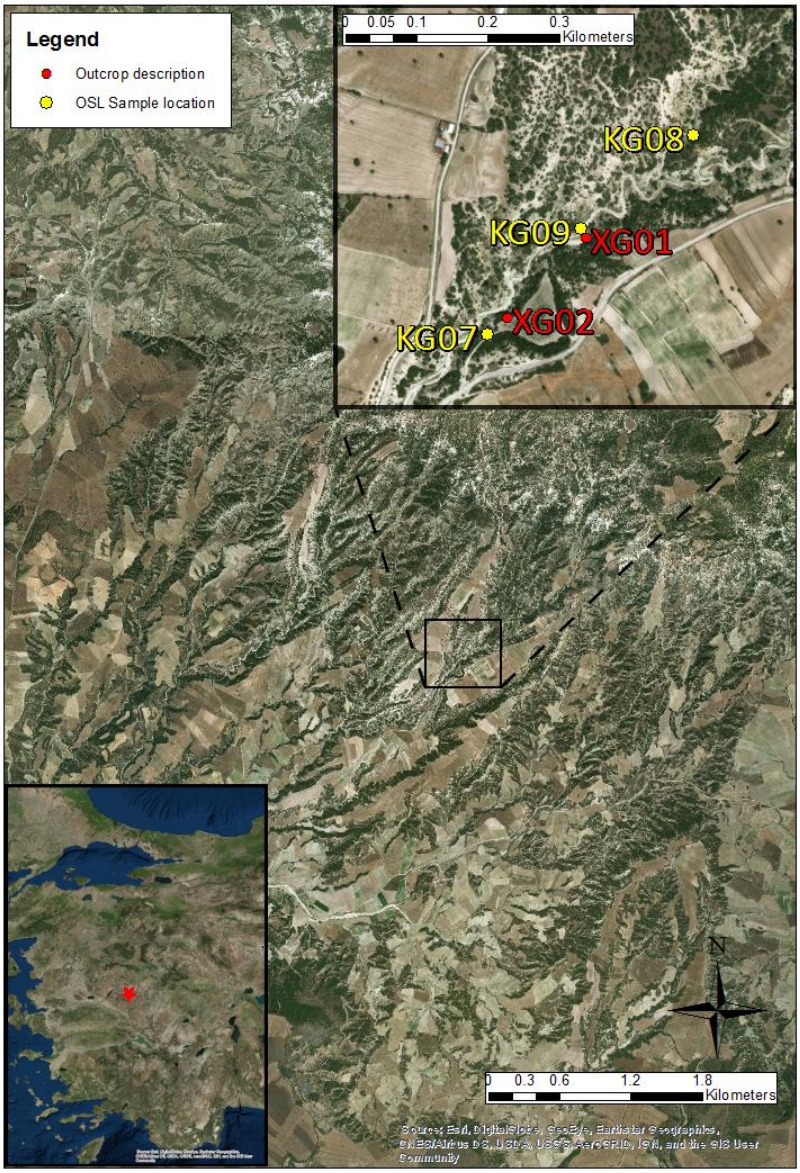

Figure 4 Aerial view of the Kula badlands, with its location on the Turkish peninsula. OSL sampling locations are shown in yellow, while the locations where additional stratigraphic descriptions were made are shown in red.

3.2.2. Preparation

Processing of the samples was done under dimmed amber light conditions at the Netherlands Centre for Luminescence dating (NCL). When opening sample tubes, the outer 3 cm were removed first since these edges are prone to light contamination during sampling. Instead, this material is used for making "pucks" which are used for dose rate measurements. The remaining sediments were wet sieved and the 212-250 μm fraction separated. The grains were treated with hydrochloric acid (HCL) and hydrogen peroxide (H_2O_2) to remove any carbonate materials and organic compounds, respectively. The quartz and feldspar minerals were separated based on their differences in density. This is achieved by using a solution (LST, p = 2.58 g/cm^3) with a density in between that of quartz (p = 2.65 g/cm^3) and feldspar (p = ~2.56 g/cm^3). The quartz fraction is further extracted with magnetic separation in which almost all magnetic minerals are removed from the quartz. A subsequent treatment with hydrofluoric acid (HF) for 45 minutes is performed to

remove any leftover feldspar and to etch the surface of the quartz grains in order to remove the alpha-irradiated part from the grains.

3.3. Equivalent dose: quartz

3.3.1. Single Aliquot regenerative (SAR)

OSL measurements of the quartz minerals were done according to the single-aliquot regenerative-dose (SAR) procedure (Murray and Wintle, 2000). With this procedure, the natural luminescence signal of a disc containing the sample grains (i.e. an aliquot) is measured and then this same disc is used for repeated cycles of irradiation and measuring. In each cycle a test dose is applied and measured so that for each cycle the change in sensitivity of the aliquots can be monitored (Rhodes, 2011). The natural and regenerative signals, after subtraction of the background signals can then be used to construct a dose response curve. A general regenerative point sequence is set up according to Table 2 (Murray and Wintle, 2003), for a more detailed version the reader is referred to appendix Table A.

Table 2 Regenerative sequence used in the quartz OSL measurements following Murray and Wintle (2003). These steps are cycled through, with each cycle being a run and the combination of cycles is referred to as a sequence. The range of beta irradiations are only from the second run onwards, whereas in the first run the natural dose is measured, which doesn't require laboratory induced irradiation. The IR-scan is only applied in the last run to measure the influence of feldspars, if present.

Step		**Description**
1	Natural dose	Natural; Beta irradiation of variable strength
2		Preheat at 200 °C
3		IR-scan, only in last run
4		Blue LED OSL measurement at 125 °C
5	Test dose	Beta irradiation of 4.1 Gy
6		Cut heat at 180 °C
7		Blue LED OSL measurement at 125 °C
8		Bleaching OSL 210 °C

An automated luminescence reader was used for measurements (Risø TL/OSL DA-20). This reader was equipped with a $^{90}Sr/^{90}Y$ beta source (Bøtter-Jensen et al., 2000) which at the time had a dose rate of 0.0821 Gy/s. The dose rate of the source is checked every month and since the measurements span a period of two months there is a slight decrease in dose rate visible, down to 0.0818 Gy/s. About half of the disc of samples NCL1218129, -130 and -132 were calculated using this decreased dose rate. As can be seen from Table 2, blue LEDs with a U-340 filter were used for stimulation of the quartz grains.

3.3.2. Measurements

Prior to equivalent dose measurements tests were conducted to examine the suitability of the quartz minerals for luminescence dating. A sequence using a single regenerative point alongside a zero dose and two recycling doses, of which one contained an IR-scan, was carried out on all five samples. The measurement was done using 3 mm aliquots, 3 discs per sample, while preheat temperatures were set at 220 °C for 10 s. Preheating of the aliquot is done to remove unstable signal components (Rhodes, 2011).

This resulted in one sample (NCL-1218128) not giving any useful signals, mainly because of contamination by feldspar minerals (Figure 5). The other four samples (NCL-1218129 - 132) were used in the quartz equivalent dose measurements.

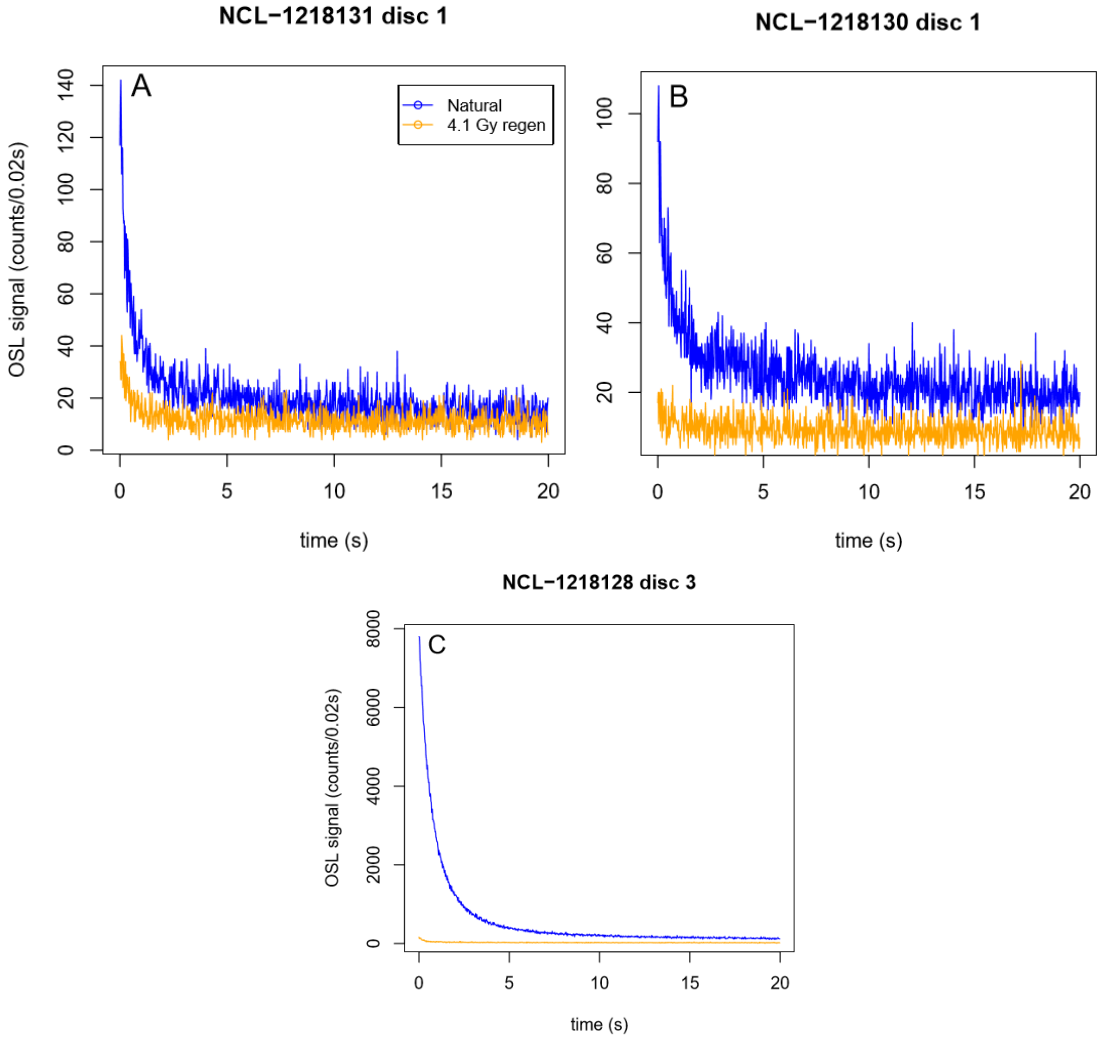

Figure 5 Typical OSL curves of (A) a suitable quartz sample, (B) a sample rejected because the test dose error exceeded 25% and (C) a sample contaminated with feldspar. The blue curve are the natural signals measured, while the orange curves are measured in a regenerative run of 4.1 Gy.

Prior to the equivalent dose measurements several performance tests were performed. The first test was a combined dose recovery and preheat plateau (php) test. This combination was necessary so the variation between the different preheat temperatures would not be caused by the natural variation within the sample. This way, the temperature at which the OSL signal is most stable and where there is minimal influence of unwanted signals can be determined (Wintle and Murray, 2006). The test was done using aliquots of 3 mm from a single sample (NCL-1218132) with 4 aliquots per temperature. After bleaching, the aliquots were irradiated with a dose of ~6.2 Gy and three regenerative points were measured; 4.1, 8.2 and 16.4 Gy. Also, a zero dose and the two recycling doses are measured similar to the equivalent dose measurements except now adjustments are made to fit the preheat plateau test. An overview of the steps

taken can be found in appendix Table B. The preheat plateau test was performed between 180 and 280 °C (Cut heat 20 °C lower with a maximum of 220 °C) and a plateau is clearly visible between 200 and 240 °C (Figure 6).

Furthermore, a thermal transfer test was performed to see at which temperature there is an extra signal due to charge being transferred from heat sensitive traps to light sensitive traps (Wintle and Murray, 2006). This is especially important for young samples where it has comparatively more influence on the final dose estimation (Wintle and Murray, 2006). For a generalised sequence of the thermal transfer test the reader is referred to the appendix Table B. When putting the results of the php-test and the thermal transfer next to each other, it seems that at a temperature of 200 °C both the thermal transfer is at a minimum and the signal is most stable (Figure 6). For these reasons it was determined that all quartz equivalent dose measurements would use a preheat of 200 °C and a cut-heat of 180 °C.

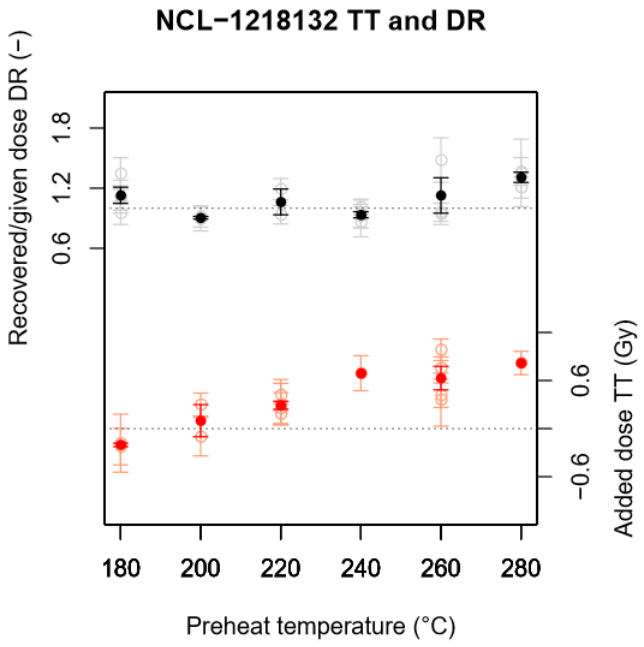

Figure 6 Preheat plateau (top; black) and thermal transfer (bottom; red) performance test results. The horizontal lines indicate unity for the dose recovery and zero for the thermal transfer data. The faded points are the individual values, whereas the solid, more opaque colours indicate the average over these points. The lack of error bars in the averaged values is caused by the fact that the point consists of a single value Therefore, the error of the individual point has to be used in that case. Thermal transfer was not accounted for in the dose recovery ratios.

Take note that of the four aliquots per temperature not all passed the rejection criteria described below. This means that the amount of actual data points is limited and even reduced to one in some cases. Partly because of this, another dose recovery test was performed, this time for all four samples with a preheat of 200 °C, as an extra precaution for the validation of the method. The dose to be recovered was 4.1 Gy. This relatively low dose is taken to simulate the expected young ages. Regenerative points were measured at ~5 and ~9.8 Gy with a zero dose and two recycling doses of ~5 Gy (appendix Table A). Although small differences are noticeable, all samples recover the dose to a large extent. The average recovered doses are 4.5, 3.7, 4.2 and 4.7 Gy for samples NCL-1218129, 130, 131 and 132, respectively. This translates to

recovered/given ratios of about 1.1, 0.9, 1.0 and 1.1, which do approach unity (Figure 7). Therefore, it can be said with relative certainty that using a preheat temperature of 200 °C is a suitable strategy.

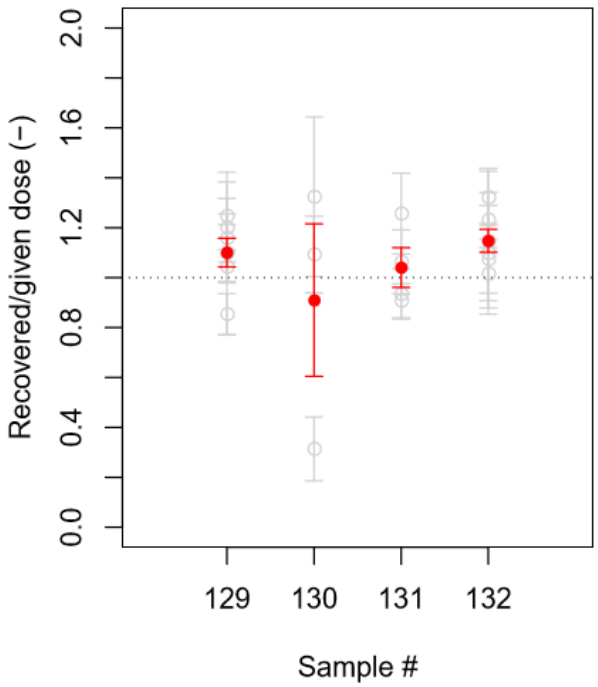

Figure 7 Results of the separate dose recovery test for the four quartz samples. The transparent points and error bars are the individual measurements, the red ones are the averaged values.

Equivalent dose measurements follow a similar procedure as the first equivalent dose test measurement. In order to save time a base sequence was constructed which could be extended with additional regenerative points. This base run consists of one regenerative point of ~4.1 Gy, a zero dose and two recycling doses, as was done before which of course includes the measurement of natural and test doses. The test dose was set to ~4.1 Gy.

The results from this base run were used to determine which discs gave proper signals and whether the measured signal exceeded the 4.1 Gy regenerative point. If this was the case, additional regenerative points of 8.2, 16.4, 41.0 and 123.1 Gy were measured. Dose estimations of these extended runs were obtained by fitting an exponential function (in "Analyst 4.31.9"; Duller, 2015), whereas dose estimates based on the base run were obtained by fitting a linear function. Error calculations were done using Monte Carlo with 1000 repeats in "Analyst". Exceptions were made where it would be more efficient to run the complete sequence at once, thus fitting an exponential function with low dose estimates. Equivalent doses should be calculated from the "fast" component of the OSL decay curve (Murray and Wintle, 2003; Wintle and Murray, 2006). This signal is preferred due to its stable, easy to bleach characteristics (Wintle and Murray, 2006; Cunningham et al., 2011). The less suitable slower OSL components are minimised with an "early background" approach. Cunningham et al. (2011) demonstrated that with the early background approach samples were less affected by thermal transfer and showed less recuperation. Thus, the integration limits of the initial signal are set to channels 1-24 (0.02 - 0.48 s, with step size of 0.02 s) and the early background subtraction is bounded by integrals 25-88 (0.50 – 1.76 s). The aliquots that were

within 25% of the recycling ratio, within 25% of the max test dose error and where the recuperation was smaller than 10% of the largest regenerative dose, were accepted for further analysis. These criteria are relatively lenient, but due to the poor performance of the grains they were considered to be acceptable.

3.3.3. Aliquot size

The expectation was that there would be a large spread in numerical ages due to a large variability in bleaching times. Therefore, it is preferred to measure at a single-grain level so that well bleached fraction can be isolated. However, it is much more efficient to measure quartz with aliquots instead of single grain since the percentage of grains that give a sufficient signal is much lower compared to feldspar (Duller et al., 2003). However, with multi-grain aliquots there is a risk of averaging the D_e signal when the size of aliquots becomes too large (Duller, 2008). Averaging can result in overestimation of the age, especially in this case where a lot of grains are poorly bleached. Therefore, the aliquot size that still can serve as a proxy for genuine single grain measurements needs to be established. For this we need to examine what percentage of grains contribute to the luminescence signal. To achieve this, a single grain quartz measurement was carried out for two different samples (NCL-1218131, -132). Here, the signals from every grain are summed and this way it can be determined how much every individual grain contributes to the overall signal (Figure 8). These "light sum curves" are constructed for both the natural signal and the test dose signal. These runs use the same sequence as multi grain sequences, though adjusted for single grain measurements. This implies single grain stimulation using a green laser instead of blue LEDs.

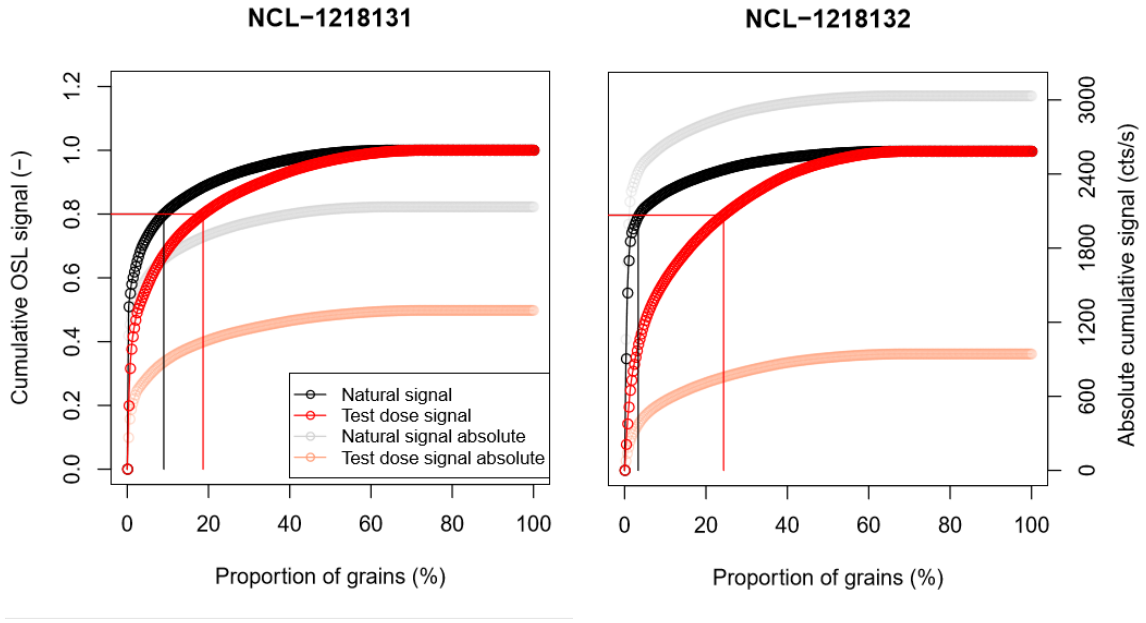

Figure 8 Cumulative light sum curves of the samples NCL-1218131 and -132. The transparent curves indicate the absolute cumulative signal in counts per second. The opaque curves are normalised to the total summed signal. Red curves stand for the test dose signal, whereas the black curves are the natural signal. Horizontal/vertical lines are drawn to indicate the theoretical percentage of grains that make up 80% of the total signal.

Comparing both samples, there is a clear difference between both, especially in the test dose. Whereas in sample NCL-1218131 80% of the total signal is produced by 9% and 19% for the natural and test dose respectively, in sample NCL-1218132 a large difference is visible with 3% and 24% for natural and test dose respectively. Although the curves of the natural dose show a curve more representative for a general

quartz signal (Duller et al., 2003), this is mainly caused by the natural variation within the sample where the older grains give a brighter signal thus overshadowing the younger grains. Therefore, it is logical to use the test dose signals. This would mean that for an aliquot of 2 mm, which contains about 49 grains, about 9 grains would make up 80% of the signal for sample NCL-1218131. For the other sample that would be 11 grains. The same procedure only with a size of 1 mm (about 13 grains) would result in about 2 and 3 grains dominating the signal for sample NCL-1218131 and -132, respectively. Ideally, about 80% of the signal should originate from 1 – 2 grains in order to approach single grain measurements (Reimann et al., 2012a), Which is almost achieved with 1 mm aliquots with these samples. However, when looking at the absolute luminescence values it becomes apparent that the signal in general are very dim (cumulative total of 600 – 1200 counts). Even with quartz one would usually expect a couple of thousand counts for the initial signal. Reason for these dim signals is probably related to a low sensitivity caused by limited reworking of the grains. This is evident from the predominantly carbonate fraction in the outcrop and the SW flow direction of the sediments, which suggests erosion from the nearby limestone plateau in the northeast in conjunction with erosion from the underlying metamorphic rocks (See section 5.1). Because the signal is so low, the number of aliquots that give a useful signal is also very low when using small aliquots. It is therefore very likely that averaging will occur, but in order to get sufficient signals within the time frame of this research it is necessary to use larger aliquots. A proper balance is found at 2 mm aliquots where about 40 - 50% of the aliquots are accepted and the youngest ages are still identifiable, compared to ~20% when using 1 mm aliquots. Furthermore, when comparing the equivalent doses of 1- and 2-mm aliquots there is no significant difference in the MAM estimate (Figure 9). The 1 mm aliquots showed less poorly bleached signals, but the well bleached signal is still recognisable with 2 mm aliquots. Because of the averaging it is reasonable to assume that the small aliquot quartz OSL ages might be slightly overestimated. Thus, the majority of aliquots were measured with a size of 2mm, with the exception of a couple of aliquots for sample NCL-1218131 which had a mask size of 1mm. Note that the equivalent doses from the 1mm aliquots are still included in the final burial dose.

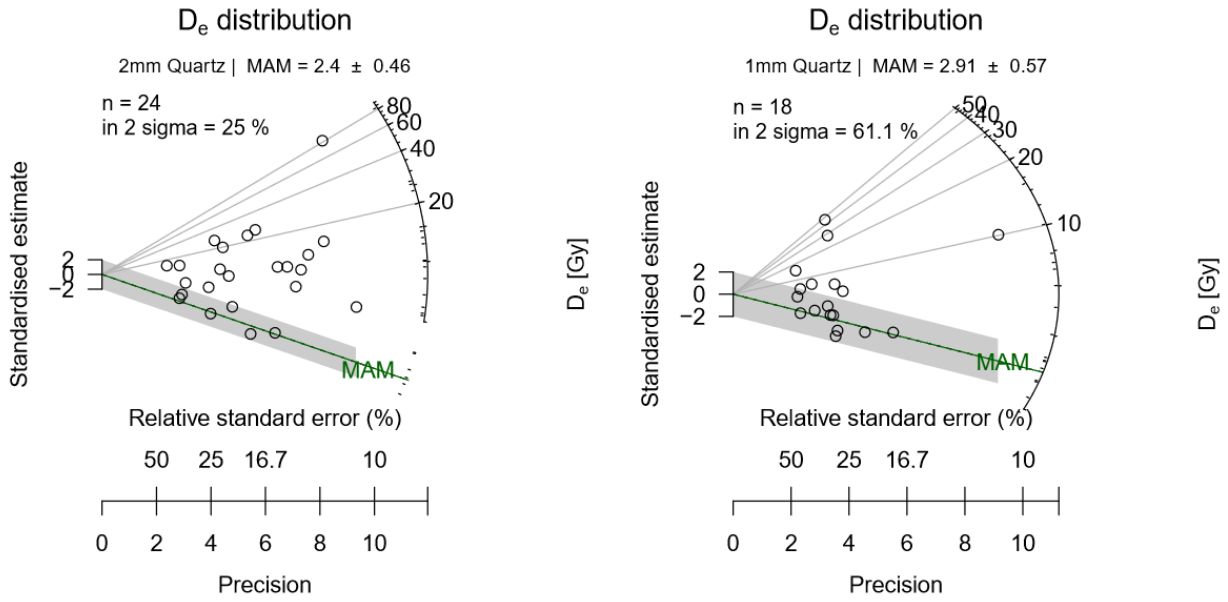

Figure 9 Equivalent dose distributions of sample NCL-1218131 when 2 mm aliquots were used (left) and when 1 mm aliquots were used (right).

3.4. Equivalent dose: K-feldspar

3.4.1. Single grain pIRIR

Instead of blue LED's, feldspar is measured using infrared stimulation (IRSL) using a similar single-aliquot regenerative protocol (Wallinga et al., 2000). Furthermore, a post-IR IR (pIRIR) procedure is adopted (Thomsen et al., 2008). This method measures two IRSL signals: one at a temperature of 50 °C and another at 175 °C. The increased temperature should minimise the effect of anomalous fading (Thomsen et al., 2008; Reimann et al., 2011) at the cost of an increased bleaching time (Kars et al., 2014). Since the expectation was that the sediments were of quaternary or even Holocene age, it was opted to take a pIRIR temperature of 175 °C to minimise the residual signal originating from possible thermal transfer (Reimann and Tsukamoto, 2012).

Whereas the quartz measurements were mostly done using single aliquots with multiple grains, feldspar measurements were done using single grain discs. The grains are loaded on discs containing holes in a 10 x 10 grid. The reader used (Risø TL/OSL DA-15) is a similar device as the one used for quartz, the difference being that for the measurements of feldspar different attachments are used to allow for single grain IR stimulation. This particular reader has the same type of beta source as the one used for the quartz measurements, only this one had a dose rate of 0.1002 Gy/s at the time of the first measurements. This value is kept fixed for all feldspar calculations since the decrease in dose rate is negligible. Stimulation of the grains was done with IR LEDs and a I-410 filter was installed in front of the photomultiplier tube. The setup of the sequence is shown in Table 3, with a more detailed description in appendix Table D.

Table 3 Regenerative sequence of the feldspar measurements adapted from (Reimann et al., 2012b)*. Modifications include a double IRSL measurement at 50 and 175 °C and the addition of bleaching steps between (test) dose measurements.*

Step		**Description**
1	Natural dose	Natural; Beta irradiation of variable strength
2		Preheat at 200 °C
3		Single grain OSL IR LED at 50 °C
4		Single grain OSL IR LED at 175 °C
5		Bleaching OSL at 175 °C
6	Test dose	Beta irradiation of 10 Gy
7		Preheat at 200 °C
8		Single grain OSL IR LED at 50 °C
9		Single grain OSL IR LED at 175 °C
10		Bleaching OSL at 175 °C

3.4.2. Measurements

The sequence for feldspar included six regenerative doses of 5, 10, 20, 40, 80 and 160 Gy of β-irradiation as well as a zero dose and a recycling dose of 10 Gy. The test dose was set at 10 Gy while preheat temperature were set equal to that of the quartz measurements, 200 °C for 60 s. All equivalent doses were

derived from fitting an exponential function to the dose response curve. To remain consistent with the quartz analysis the same rejection criteria are applied, as well as the use of the Monte Carlo simulation with 1000 repeats. Still, for feldspar different integrals have been used, channels $6-8$ for the initial signal and $40-50$ for the late background signal (step size of 0.03 s). It is opted to use a late background instead of an early background, since it is argued that the source of the signal is not comparable to that of quartz (Buylaert et al., 2012). Furthermore, the difference due to late and early background subtraction is likely negligible for feldspar equivalent doses (Vasiliniuc et al., 2013).

In order to judge the suitability of the feldspar OSL method two tests were performed; a dose recovery and anomalous fading test. Prior to the dose recovery test the sample (NCL-1218132) was bleached for two days in a solar simulator. In the sequence, the bleached grains received beta-irradiation of ~10 Gy. The settings of the sequence remained the same compared to the D_e sequence, except for the regenerative points, which were set at 7.5, 15, 30 and 60 Gy (Appendix Table D).

The same sequence also contained a residual dose measurement. No dose was applied to these bleached grains and direct measurement should, ideally, result in no signal. Since it is nearly impossible to completely reset the signal and in combination with uncertainty in the equipment, an average of 1.51 ± 0.28 Gy (n = 27) of residual dose is measured. When subtracted from the recovered dose, the average recovered dose equals to 10.16 ± 1.10 Gy (averaged over 50 doses) and is approximately normally distributed around 10 Gy (Figure 10). This shows that the applied protocol is adequate.

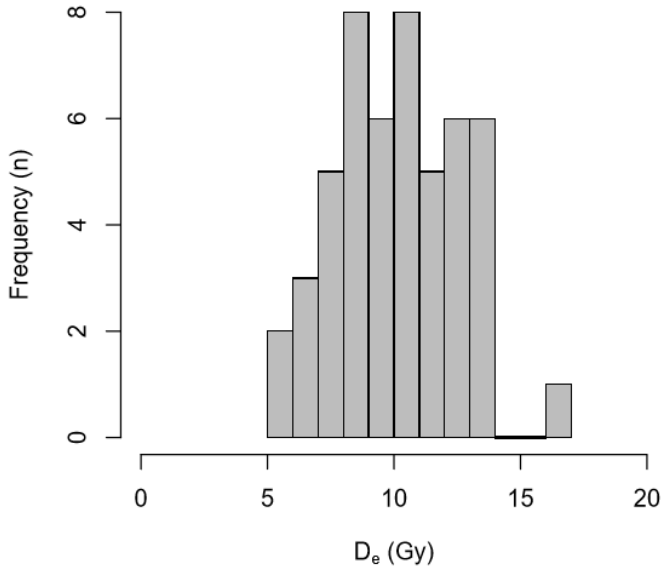

Figure 10 Distribution of the recovered equivalent doses in the feldspar dose recovery test. The applied dose was about 10 Gy.

Because the average was used in calculating the recovered dose, an averaged residual dose was subtracted. This will not hold for the equivalent dose measurement which have calculated using a MAM. Therefore, the MAM was applied to the residual doses and this resulted in a value of 0.64 ± 0.15 Gy (Figure 11). For the youngest sample this would mean that the burial dose would decrease to about 0.96 Gy which translates to an age of ~0.37 ka. This age is considered to be highly unlikely given the setting and origin of the sediments (see section 4.1). This is reason to believe that bleaching under laboratory conditions does not reflect the natural conditions of a fluvial setting, accurately. As a result, the choice was made to exclude the residual dose subtractions from the D_e calculations.

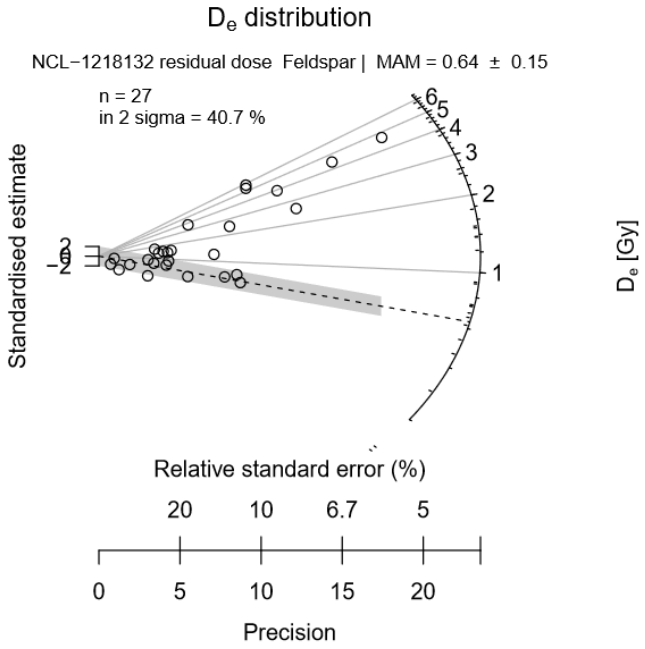

Figure 11 Distribution of the residual doses shown in a radial plot. The centrality is based on the MAM (Galbraith et al., 1999).

Anomalous fading is another process affecting age estimation leading to an age underestimation, if present and not accounted for. Although anomalous fading is minimised by implementing a pIRIR protocol at 175 °C, there is still a possibility of it being present. Therefore, a single grain fading test was performed on every feldspar sample to quantify the potential underestimation. After bleaching (by a D_e sequence before it) the grains received a dose of ~10 Gy. The sequence is constructed in a similar way as the D_e sequence but including pauses of various lengths in between irradiation and measurement. The pause intervals were set at about 0.4, 0.6, 5.3 and 53.4 hours. For every disc the results of the grains were summed. In every disc the data is quite scattered, which makes it nearly impossible to describe a trend and to extract useful information as can be seen from the two samples in Figure 12. The scatter might be explained by the overall low signal, which very rarely exceeds 1000 counts per second, and because there is most likely hardly any fading present. Though it is hard to pinpoint an exact cause. It was therefore assumed that there would be no significant influence of anomalous fading and that the pIRIR protocol would minimise this to a sufficient degree. No extra corrections were made.

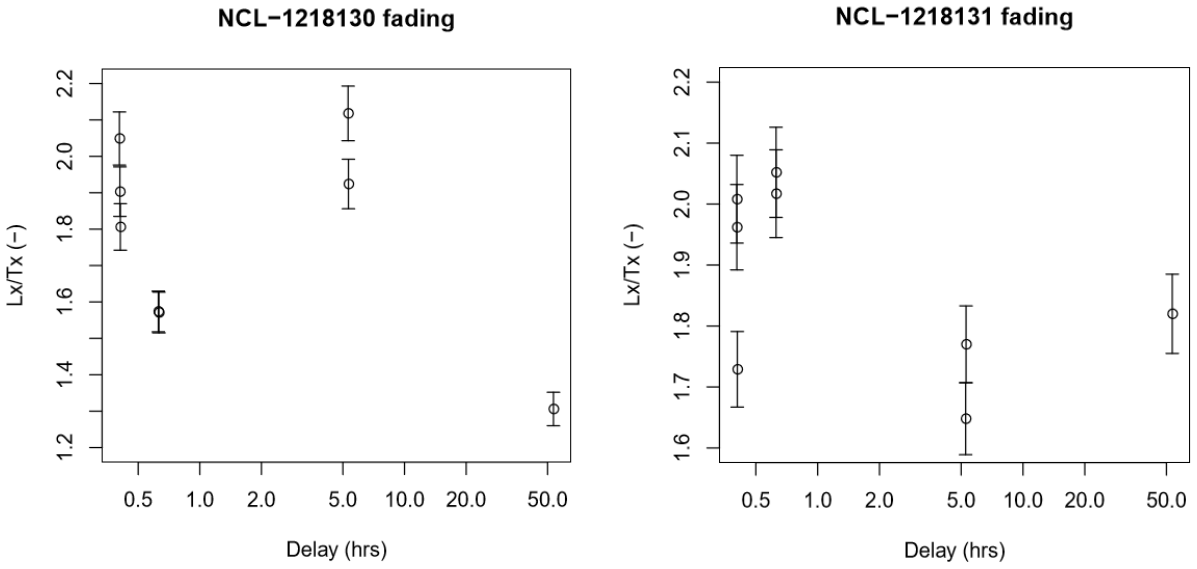

Figure 12 The results from the anomalous fading test of two of the samples; NCL-1218130 (left) and NCL-1218131 (right). The values are the result of summing 100 grains.

3.5. Dose rate

The dose rates were determined by measuring radionuclide concentrations from the sediments gathered from the outer 3 cm of the sampling tube using high-resolution gamma spectrometry. Water content and organic compounds are accounted for by drying and ashing the samples, respectively. This is needed since water and organic matter absorb radiation and thus reduce the dose rate (Lian et al., 1995; Rhodes, 2011). For the water content a value of 5 ± 2% is used which is deemed representative for the setting. The samples were taken far above the groundwater level and due to the relatively coarse-grained sediment the soil is quickly drained. Additionally, the Mediterranean climate is dry for roughly 6 months a year, so to account for the wet winters the water content is taken slightly higher compared to arid soils. The measured organic contents are used according to Table 4.

To estimate the contribution of the cosmic dose rate to the total dose rate, it is assumed that the current depth of the samples remained relatively constant since burial since there are no indications that there have been large deposits on top of the current surface. Furthermore, the assumption is made that burial was instantaneous or at least at relatively fast rates which could be considered instantaneous. Calculation of remaining variables within the dose rate (cosmic dose rate, etc.) was done according to procedures set by the NCL laboratory.

Table 4 Input parameters as they were used for the calculation of the dose rate.

Sample	**Sampling depth (m)**	**Water content (%)**	**Organic matter (%)**
NCL-1218128	3.20	5.00 ± 2.00	1.19 ± 0.30
NCL-1218129	4.50	5.00 ± 2.00	1.87 ± 0.47
NCL-1218130	4.20	5.00 ± 2.00	1.36 ± 0.34
NCL-1218131	3.00	5.00 ± 2.00	2.79 ± 0.70
NCL-1218132	2.75	5.00 ± 2.00	3.07 ± 0.77

Dose rate calculations for K-feldspar required additional calculations to account for the internal radiation of K-feldspar from the isotope ^{40}K, where we assumed an internal K-content of 10 ± 2% (Smedley et al., 2012). The resulting dose rates are shown in Table 5.

Table 5 The resulting dose rates for quartz and feldspar.

Sample	**Dose rate quartz (Gy/ka)**	**Dose rate feldspar (Gy/ka)**
NCL-1218128	-	2.49 ± 0.16
NCL-1218129	1.87 ± 0.07	2.65 ± 0.16
NCL-1218130	1.96 ± 0.08	2.75 ± 0.17
NCL-1218131	2.13 ± 0.08	2.91 ± 0.16
NCL-1218132	1.75 ± 0.07	2.54 ± 0.16

4. Results

4.1. Stratigraphy

Stratigraphic descriptions and correlations were made based on three outcrops where samples were also collected for OSL dating. In order to get the most complete picture of the landscape dynamics, two additional outcrops were described as well. These are referred to as XG01 and XG02. Although these outcrops were very well exposed, the Quaternary sediments were located high within the outcrop. Therefore, descriptions could only be made visually from a distance and based on photographs, affecting the amount of detail that could be distinguished. Nevertheless, these outcrops are vital in correlating the more detailed stratigraphy's. The outcrop locations can be found in Table 6.

Table 6 Position in UTM and lower and upper boundary of the outcrops of the sample locations as well as the locations of the additional outcrop descriptions.

Location Code	**X-coordinate (UTM)**	**Y-coordinate (UTM)**	**Bottom elevation (m a.m.s.l.)**	**Top elevation (m a.m.s.l.)**
KG07A/B	0654883	4280824	498	504
KG08A/B	0655174	4281105	502	510
KG09	0655015	4280973	503	~509
XG01	0655015	4280973	503	513
XG02	0654911	4280848	498	503

4.1.1. Observations

Location KG08 is the most upstream outcrop (Table 6; Figure 13). At this location the current incision level is about 10 m below the surface of the old plateaux level, while the bottom of the outcrop is about 6 m above the current gully level. A clear sedimentary succession can be observed. At the bottom 5 m of the sedimentary succession a homogeneous, light brown-yellowish layer is present, which consists of very fine-grained sandstones (unit M). Within this layer a normal fault is observed with a dip angle of 56° and a dip azimuth of 36° (not visible on the photograph). This layer is unconformably overlain by a layer of relatively poorly sorted, mostly carbonate pebbles in a sandy matrix (Fc3). The pebbles and cobbles are angular and reach diameters of 10 cm. Though not very clear, imbrication of the pebbles seems to indicate a flow direction towards the SW. This layer is followed by a 30 cm thick, layered, but discontinuous layer of fine-grained sandy material (LF2). The subsequent unit (Fcb1) shows a completely different, more chaotic environment. Large angular boulders up to 30 cm in diameter are relatively poorly sorted, but the flow direction is discernible following a NNE-SSW direction (~202°). Besides the predominantly carbonate pebbles, pebbles of basaltic origin can also be found. They are rounded and relatively small (up to 2 cm in size). The unit is partly overlain by a coarsening upward sequence of clayey to sandy material (LF3). Based on the grain size, about three thin subunits can be detected in this sedimentary unit, which indicates a slight increase in fluvial energy during deposition. The remaining upper 2 m of the outcrop consists of fine-

grained material with rare angular carbonate pebbles. As can be seen from Figure 13 part of the units is positioned as a lens between the upper and lower units.

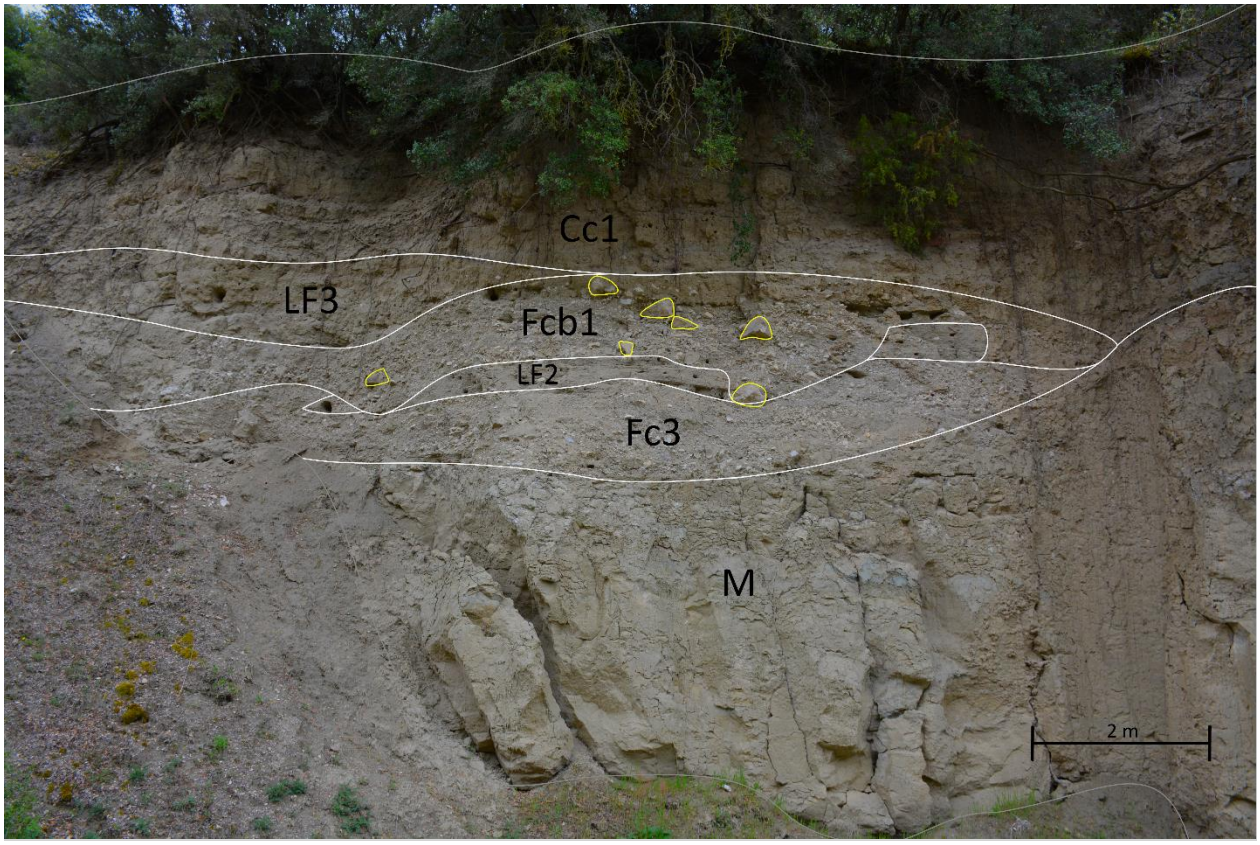

Figure 13 Photograph of outcrop KG08 with the delineated units. Yellow lines indicate clasts which are over 30 cm in diameter. The outcrop can be found at UTM coordinates 35S 0655174 E, 4281105 N. The orientation of the photograph (and the outcrop) is 120°.

A similar sedimentary succession can be found downstream at location XG01. Due to the inaccessibility (Figure 14), thin units and (small) grain sizes could not be differentiated. The thickness of this outcrop is up to 12 meters, of which about half consists of very fine-grained sandstones (M). It is a yellowish, homogeneous layer with a lens of coarser grained material which is well layered and has a greyish colour. On top of this unit an erosional boundary is visible which is followed by a layered structure of fine and coarse sediments (Fc2). The following unit is more homogenous and about one metre thick (LF1). The subsequent sedimentary unit (Fc3) consists mainly of white sub-angular pebbles and cobbles up to 20 cm in diameter bounded by a sand and/or clay matrix and given the geological context they are likely of carbonate origin. It is estimated that the flow direction is roughly SW, but no numerical values could be assigned. This layer is followed by a layer consisting mostly of sub-angular boulders (≤ 50 cm in diameter; unit Fcb1). Again, there appears to be only carbonates material in this unit with a flow direction similar to

the units below. Also in this location a poorly sorted unit of fine material with some pebbles is found on top (Cc1).

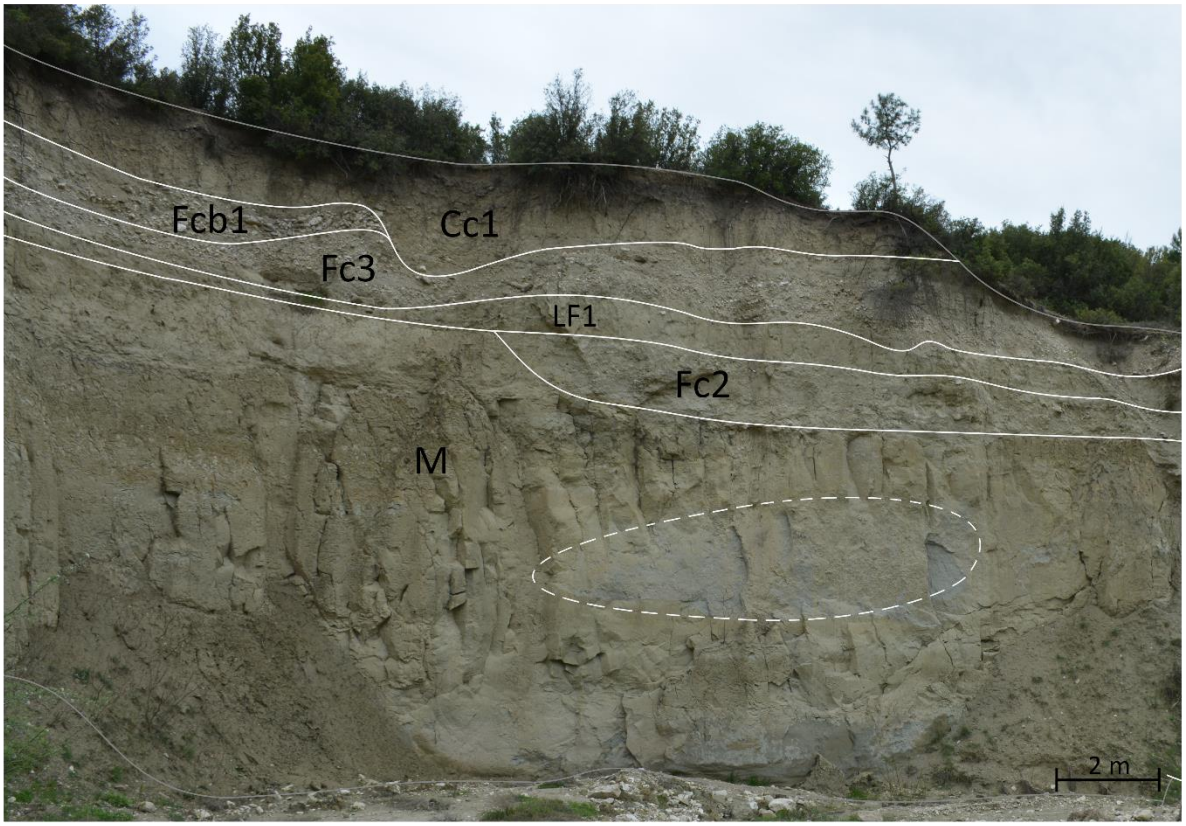

Figure 14 Photograph of outcrop XG01 with the delineated units. Dashed lines indicate relicts of other fluvials. The outcrop can be found at UTM coordinates 35S 0655015 E, 4280973 N. The orientation of the photograph (and the outcrop) is 136°.

On the other side of the gully is location KG09. The sedimentary units at sample location KG09 exhibit different physical properties in comparison to other sedimentary units described on previous locations. The orientation of the outcrop is positioned in such a way that the part exposed is perpendicular to the flow direction of the various channels (Figure 15). In total, nine different sedimentary units can be identified. Each unit displays a different composition of pebbles of carbonate, basaltic and/or metamorphic origin. Furthermore, large differences in grain and clast size are observed. A summary of the different properties can be found in Table 7 (For clarity the units are named according to the classification of section 4.1.2). Additionally, a fault can be observed in the bottom sedimentary unit which does not extend into the overlying units (Figure 15). The dip azimuth of this fault is 355°, while the dip angle is 45°.

Table 7 Summarised description of the sedimentary units at location KG09.

Unit	Matrix grain size	Thickness (cm)	Lithology	Clast max size (cm)	Roundness	Sorting
M	Very fine	>200	Sandstone	-	-	Well
Fcm1	Coarse	~200 - 300	Carbonate	~4	Subrounded	Well
			Metamorphic	~4	Rounded	
Fcb2	Coarse	~200 - 300	Carbonate	~70	Subrounded – Angular	Poor
			Basalt	~5	Rounded	
Fc4	Very coarse	~100	Carbonate	~30	Angular	Poor
Fcbm1	Fine	~50	Carbonate	~20	Subangular	Some
			Basalt	~5	Rounded	
			Metamorphic	~2	Rounded	
Fcm2	Coarse	~50	Carbonate	~30	Rounded - Subangular	Some
			Metamorphic	~2	Rounded	
Fcbm2	Coarse	~150	Carbonate	~30	Subangular	Some
			Basalt	~5	Rounded	
			Metamorphic	~5	Rounded	
Fc6	Fine	~300	Carbonate	~10	Angular	Well
Cc2	N/A	>100	Carbonate	N/A	N/A	Poor

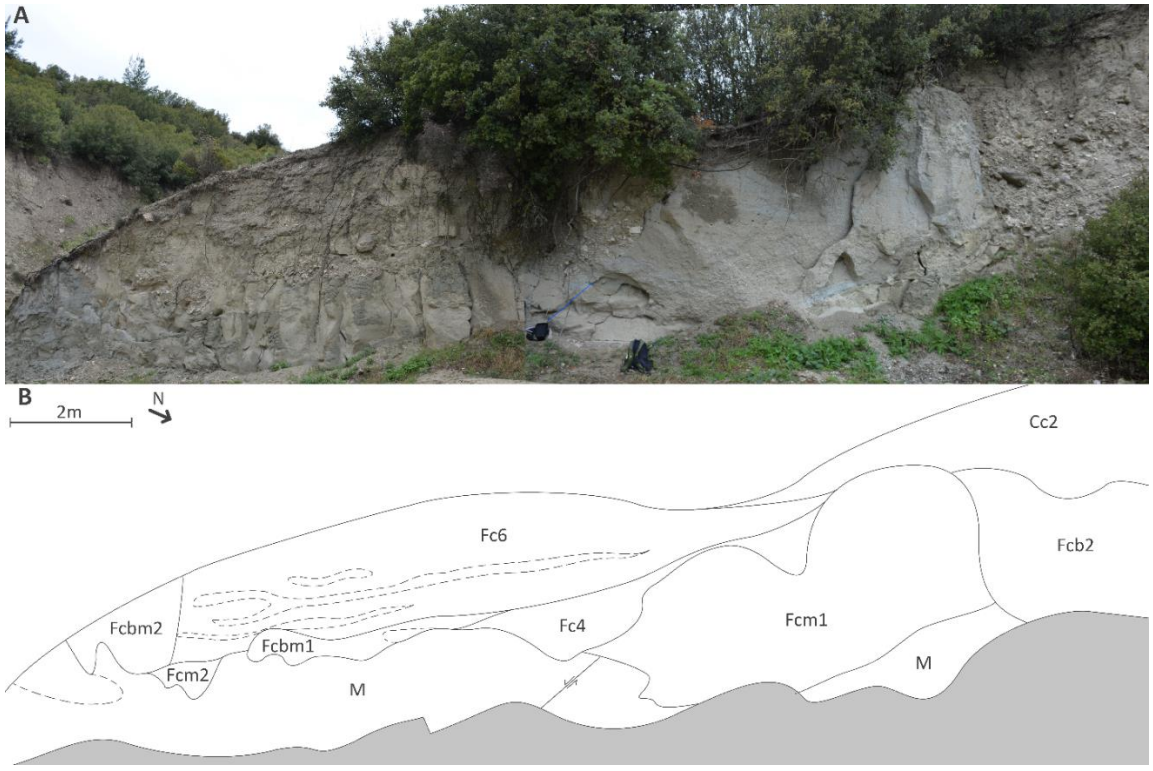

Figure 15 (A) Photograph of outcrop KG09 with the corresponding units and channels that can be distinguished. Dashed lines indicate relicts of other fluvials. At the bottom centre a normal fault is shown which orientated at 355° under an angle of 45°. The outcrop can be found at UTM coordinates 35S 0655174 E, 4281105 N. The orientation of the outcrop is 246°.

Further downstream is location XG02, which has a total thickness of about 5 m. Here, a homogeneous layer of very fine-grained sandstones is found at the bottom, followed by a layer of coarser sediments. This layer is well sorted and layered with a different colour compared to the surrounding layers. It is followed by a repetition of the bottom-most layer. This all is unconformably overlain by a unit of poorly sorted carbonate clasts up to 40 cm in diameter (Figure 16; Fcbm1), possibly containing also metamorphic and basaltic pebbles. It is positioned as a channel between the sediments of previous units. On the western side of the channel the larger pebbles and boulders are more abundant compared to the eastern side. Though unable to precisely quantify, also here the flow direction appears to go in a SW direction. On top of this layer is a channel visible with at the centre coarse carbonate material which is well sorted, which gradually transitions into finer-grained, more homogeneous deposits on both sides (Fc5). This is most likely a period of gradual deposition, where the coarse material is limited to the channel gulley with occasional flooding of the banks where fine-grained sediments were deposited. Whether this unit is continuous to the surface or another layer can be found on top is unclear due to the presence of a dense vegetation cover (Figure 16).

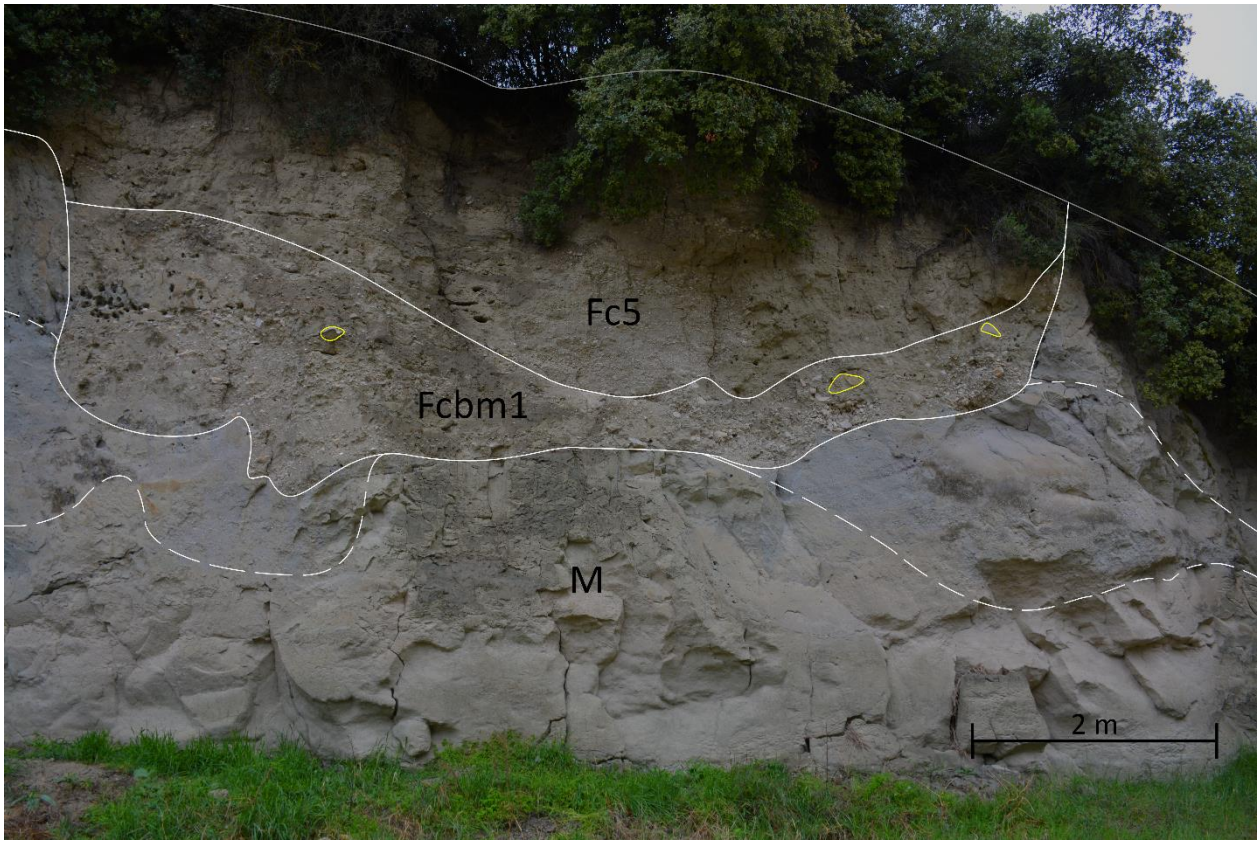

Figure 16 Photograph of outcrop XG02 with the delineated units. Yellow lines indicate clasts which are over 30 cm in diameter and dashed lines indicate relicts of other fluvials. The outcrop can be found at UTM coordinates 35S 0654911 E, 4280848 N. The orientation of the photograph (and the outcrop) is 166°.

Location KG07 is the most downstream outcrop, which is about 6 m thick. The lower most unit is a grey, layered unit consisting of coarse-grained sediments of sandstone origin. It makes up about 2 m of the entire outcrop and the top is clearly eroded (Figure 17; unit M). The subsequent unit is relatively thin (~30 cm) and consists predominantly of coarse-grained, poorly sorted clasts (≤ 20 cm in diameter) of carbonate origin within a sandy matrix (Fc1). This is followed by a relatively thick (up to 150 cm), well sorted deposit

consisting of only carbonate material (Fc2). However, compared to other units, the carbonates of this unit and the underlying unit are more rounded. A one metre thick unit (LF1) follows, which is relatively homogeneous and consists of fine-grained sandy material, indicative of a period of low energy flow. However, the flow direction is for this unit and the underlying ones undiscernible. The next overlying unit (Fcb1) consists mostly of clasts with sizes up to 50 cm. A thin, sandy lens is visible in this unit which is likely a sub-channel possibly formed synchronously or post-deposition of the surrounding unit. Alongside the pebbles of carbonate origin only a few well-rounded, pebbles of basaltic origin are found. These are well rounded pebbles not larger than ~2 cm. The imbrication of this layer is measured at 236°. It is also within this layer that a vase handle was found. Based on the material, colour and style of the handle it was estimated to be of Lydian or Hittite origin (S. Aksay, personal communication). The final layer is mostly sandy with some scattered carbonate pebbles (Cc1).

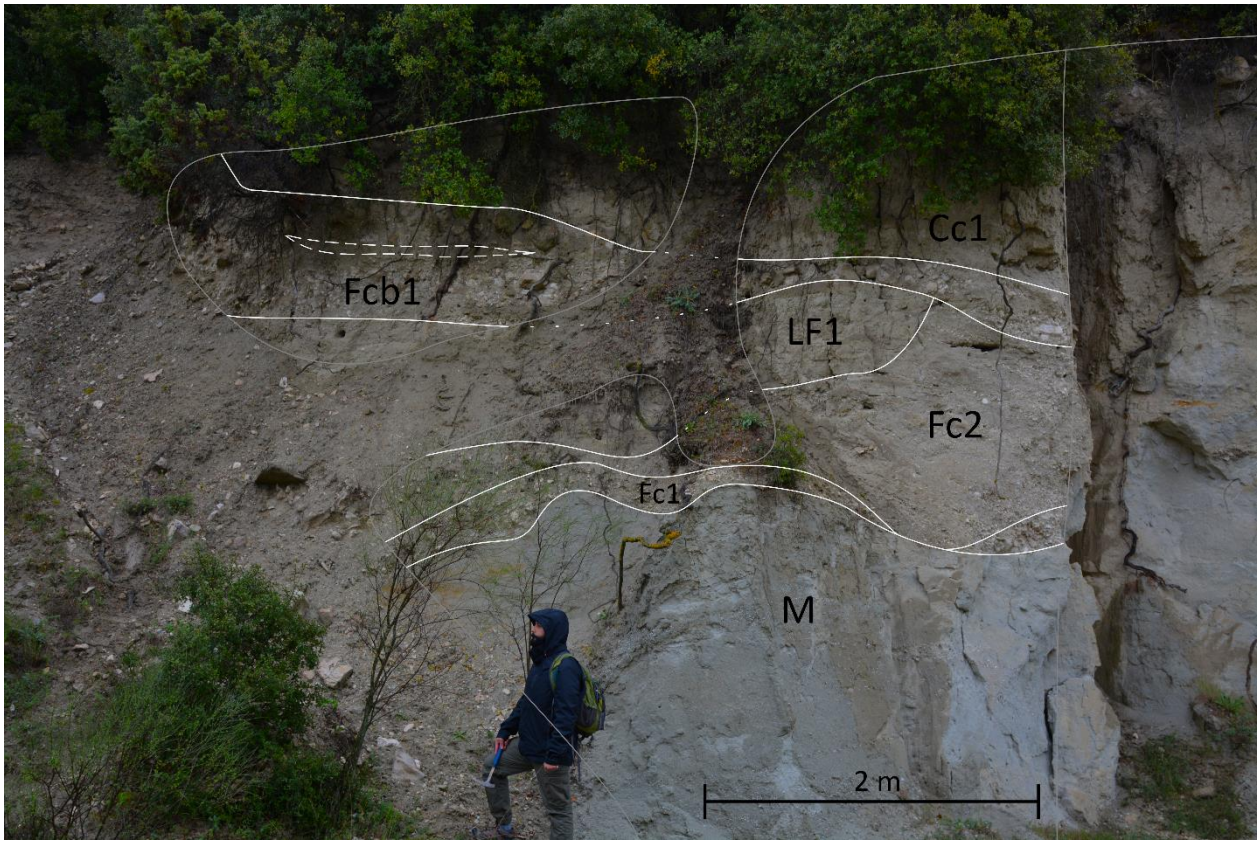

Figure 17 Photograph of outcrop KG07 with the delineated units. Dashed lines indicate relicts of other fluvials. The outcrop can be found at UTM coordinates 35S 0654883 E, 4280824 N. The orientation of the photograph (and the outcrop) is 148°.

4.1.2. Classification

Almost all sedimentary units contain carbonate clasts of different sizes within their matrix. In all cases these are either sub-angular or angular. This would suggest that these carbonates originate from the nearby Limestone plateau because the short travel distances did not allow for sufficient abrasion. Though mostly in the form of limestone, the carbonates can also be found in the form of low-grade marble or as well-developed calcite crystals. What strikes, is that KG09 shows quite a lot of lithological differences. Whereas at location KG07 and KG08 basaltic pebbles are uncommon, it is more abundant at KG09. Furthermore, metamorphic pebbles are completely absent from KG07 and KG08. The origin of the basaltic

pebbles is related to one or multiple of the volcanic events in the region. Given their rounded shape they either come from farther locations and/or they experienced multiple cycles of transport. Because of the lithological differences of the KG09 units it is not possible to correlate them with the units of KG07 and KG08. Instead it is opted to classify them separately. This is further supported by the position of the sedimentary units as they are positioned closer to the current gully level compared to the other locations. Furthermore, the relative position in the landscape suggests a disconnection between locations KG07, KG08 and XG01 on the one hand and KG09 and XG02 on the other. Since the sedimentary succession of KG09 and XG02 cannot be found underneath the sedimentary units of the other locations and since they are positioned lower in the landscape, it is likely that they have formed after the development of units at the other locations. As such, in the classification they are indicated as the younger units.

Though not obvious for every sedimentary unit, most units display a flow direction and/or layering suggesting that they are deposited by fluvial processes. This occurred at different intensities and will be classified as such; *F* for fluvial deposits with clasts and *LF* for fluvial deposits with only sand-sized material or smaller. The poorly sorted colluvial deposits are assigned a *C*. Further classification is based on the origin of the clasts and assigned a lowercase letter for the respective type; carbonate (c), basaltic (b) and/or metamorphic (m) origin.

Moreover, each sedimentary succession has at the bottom a unit with material consisting of sandstones which are either yellowish brown or grey of colour. These are considered to be part of the same unit, since the coarser, grey deposits with fluvial indications can be found as a lens within the finer grained yellow sediments. This unit is at least several metres thick and bears great resemblance to the Miocene Ahmetler Formation (Ercan et al., 1983; Ersoy et al., 2010). For this reason, this unit is considered to have been formed during the Miocene and therefore assigned the code M. With this classification it is now possible to correlate every unit and assign them a code of which the result can be found in Figure 18.

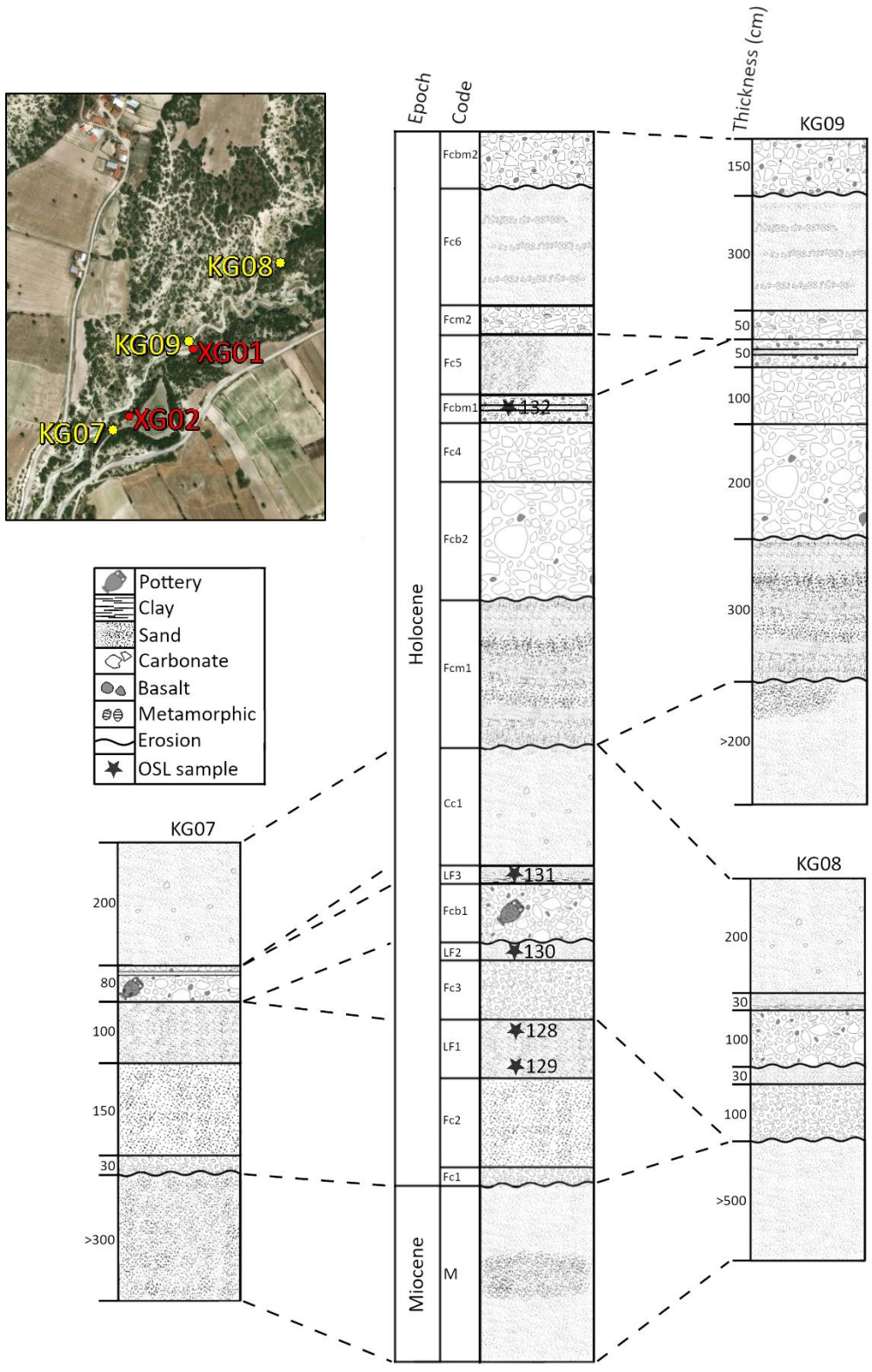

Figure 18 Stratigraphy of mapped sedimentary units with OSL ages indicated for the related units. Physical properties (grain size, lithology) are also indicated.

4.2. K-feldspar luminescence

With the choice of 2 mm aliquots, several sequences were run achieving a minimum of 40 measured aliquots per sample. What is immediately clear from the radial plots is that there is a large spread in equivalent doses (Figure 19). This is in line with the expectations of the badlands where transport distances are short and the chance of proper bleaching is limited. This is furthermore illustrated by the high overdispersion values (88 – 107%) which were calculated with the Central Age Model (Galbraith et al., 1999) and represents the scatter in the D_e distributions that is not explained by the assigned individual uncertainties. Knowing that the youngest samples will be most representative of the burial age, it was decided to apply a minimum age model (MAM) (Galbraith et al., 1999) to the data. The input parameter sigma-b, indicative of the overdispersion in well-bleached samples (Cunningham and Wallinga, 2012), for single grain quartz measurements is usually set around 20%. However, with multiple grains a correction has to be made to account for averaging. Assuming roughly 50 grains per disc and adhering to the findings by Cunningham et al. (2011), it was determined that an overdispersion of 15% is a reasonable estimation for quartz multi-grain OSL.

In general, the well bleached fraction can be identified by the MAM. However in sample NCL-1218132 there is a comparatively low dose of 0.7 Gy measured. Whether this point can be considered an outlier is debatable. Yet, there are no indications that this might have been caused by errors in the measurement protocol. With that in mind, this value is taken into the calculations of the burial dose. The possibility might still exist that the actual burial age is either higher or lower depending on whether this point is considered an error or closer to reality, respectively.

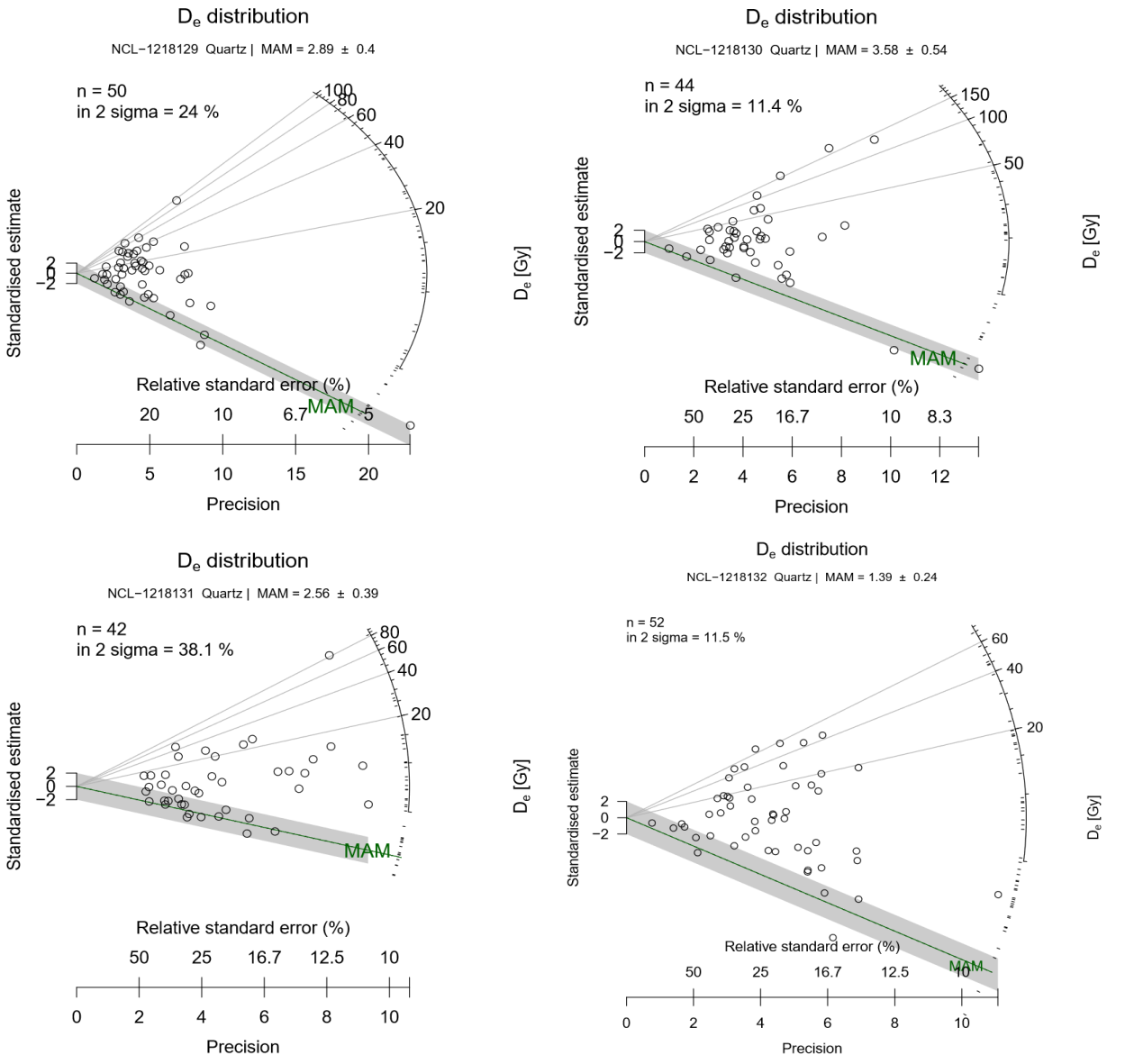

Figure 19 Radial plots of the equivalent dose distributions of the four quartz samples. Centrality of the plots are calculated using the MAM (Galbraith et al., 1999)*, with input parameter sigma-b set at 0.15. The plots were made using the R-luminescence package in R* (Kreutzer et al., 2018).

4.3. K-feldspar luminescence

The feldspar radial plots show similar characteristics as the quartz plots, namely that there is large variation in equivalent doses and therefore ages (Figure 20). This becomes even more apparent because of the larger sample population. With a more generalised view of the radial plots there appears to be a tendency towards the younger ages. Because of this and for the same reasons as is explained with quartz, a MAM is applied to the data. The input parameter sigma-b is calculated from the intrinsic overdispersion, which is derived from the dose recovery data (~23%), and an extrinsic part. This extrinsic factor is assumed to be 15% and can be summed quadratically with the intrinsic value to obtain sigma-b value of ~27%. Additionally, since feldspar takes longer to bleach than quartz (Godfrey-Smith et al., 1988) and quartz already shows a lot of poorly bleached grains, the same or worse can be expected from feldspar. This is what can be observed from the radial plots. Although on average more grains are within the MAM estimate compared to quartz. The slower bleaching rates of feldspar are also apparent from these plots as the maximum dose observed is up to ten times higher than the maximum observed doses of quartz.

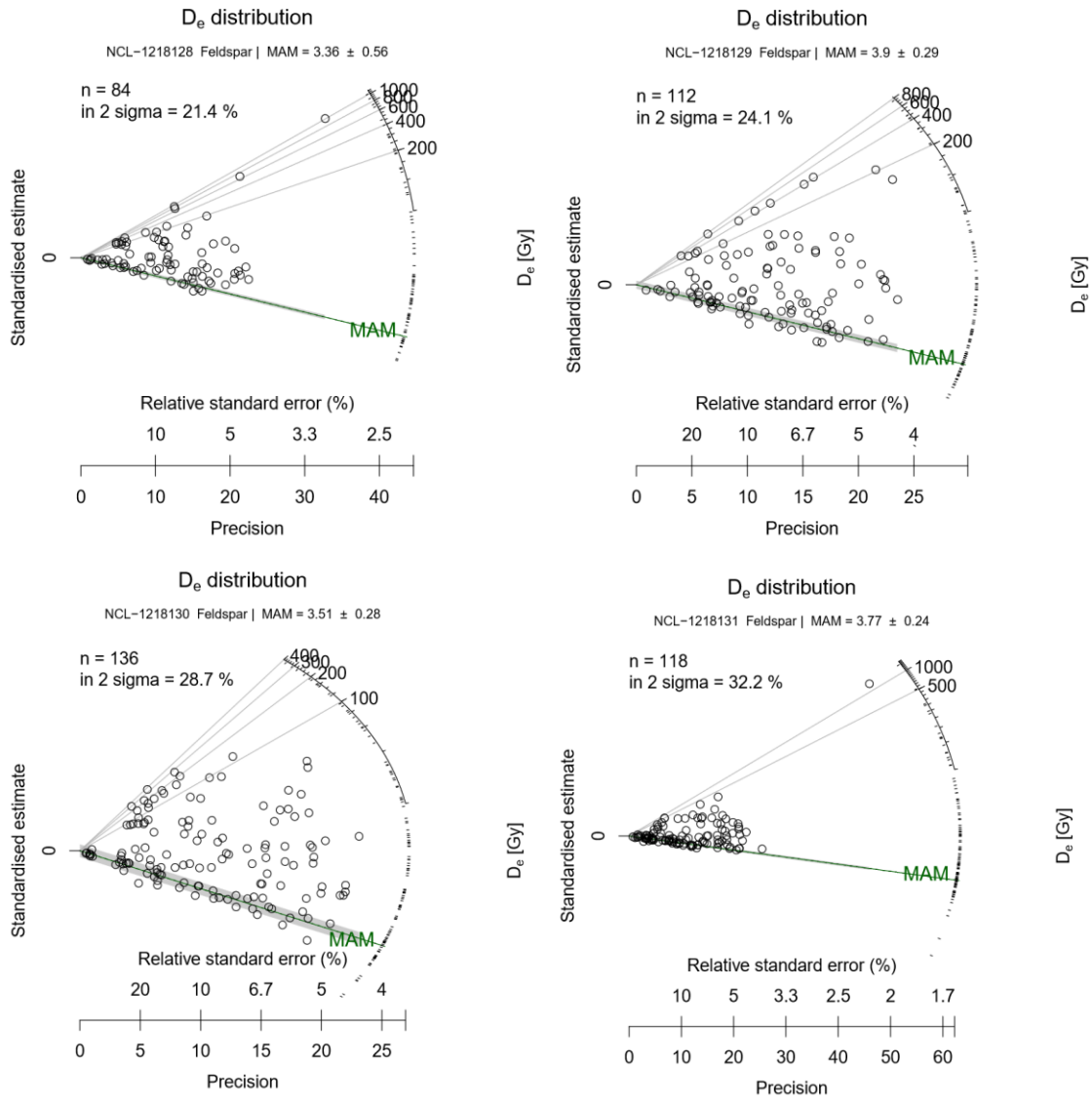

Figure 20 Equivalent dose distributions of all five feldspar samples. Centrality of the plots are calculated using the MAM (Galbraith et al., 1999). *The plots were made using the R-luminescence package in R* (Kreutzer et al., 2018)*, with input parameter sigma-b set at 0.27.*

All the MAM estimated doses, for both quartz and feldspar are summarised in Table 8. These values are divided by the dose rates mentioned in Table 5 to obtain numerical ages estimations.

Table 8 The MAM burial dose estimations and the ages based on these doses in ka before 2019. Errors are given as the 1σ error.

Sample	**Quartz MAM estimation (Gy)**	**Feldspar MAM estimation (Gy)**	**Quartz age (ka)**	**Feldspar age (ka)**
NCL-1218128	-	3.36 ± 0.56	-	1.35 ± 0.24
NCL-1218129	2.89 ± 0.40	3.90 ± 0.29	1.55 ± 0.22	1.47 ± 0.14
NCL-1218130	3.58 ± 0.54	3.51 ± 0.28	1.82 ± 0.28	1.28 ± 0.13
NCL-1218131	2.56 ± 0.39	3.77 ± 0.24	1.20 ± 0.19	1.29 ± 0.11
NCL-1218132	1.39 ± 0.24	1.60 ± 0.30	0.79 ± 0.14	0.63 ± 0.12

5. Discussion

5.1. Surface dynamics

Of the units of locations KG07, KG08 and XG01 there was one unit which appeared at all three locations, which was unit Fcb1. It is a unit about 50 – 100 cm thick with fluvial indications and clasts up to 50 cm in diameter. It is the only unit within these three locations where there are basaltic pebbles present. It is assumed for XG01 that they are present, given the similarities with the other locations. Using this unit combined with the units which were found at only two locations (i.e. LF1 and Fc2 at KG07 and XG01 and Fc3 at KG08 and XG01) it was possible to order them.

The complete sedimentary succession (Figure 18; middle) starts at the bottom with the sandstones of the Ahmetler formation which can be found at every location. This is the only unit in which faults could be observed. It is likely that these had some influence on the deposition and erosion of the overlying sedimentary units. However, both locations where the faults were observed show differences in the orientation of the fault compared to the flow direction of the overlying sediments. At KG09, the fault plane is angled ~109° to the flow direction (horizontally) while at KG08 this is almost 180°. It might be due to the fault that the sedimentary succession formed as a lens at KG08, though there are no further indications that point at that direction. At KG09 the flow direction is almost perpendicular to the fault plane suggesting the fluvial regime was influenced by the topographic differences caused by the fault. It is unclear if these faults had a larger influence on the developments of the badlands. In each case this Ahmetler Formation is followed by an unconformity. What followed is a period of more intense fluvial activity which gradually decreased. This is shown by the transition of cobble-sized carbonates (Fc1) towards a more sandy matrix with pebbles (Fc2) and eventually a completely sandy unit (LF1). The fact that only carbonate pebbles have been found, indicates that erosion is mainly from the limestone plateau. The transition to a predominantly sand-sized fraction might be due to decrease in energy or a shift from incision of the Ulubey to the Ahmetler Formation. Note that this succession is not found in the upstream location KG08 from which it might also have eroded. These units are followed by a similar trend in deposition, which starts with a roughly one metre thick unit consisting of carbonate cobbles up to 15 cm in diameter. Percentage wise this unit contains more clasts (~50%) than Fc2 (~70%) but less than Fc1 (~20%). This change in fluvial sediment input is indicative of an increase in moisture which caused more erosion, possibly in combination with a transgression into the Ulubey Formation. This unit is conformably overlain a thin sandy layer and this combination can only be found at location KG08, which is upstream. The subsequent unit is Fcb1 which is described above. Surprisingly, at location KG08 it is located above an erosional boundary, while this is

not visible at the other locations. This is likely because of the high energy flow (transport of large boulders) that eroded the underlying sandy layer, signifying the synchronous deposition and erosion. A coarsening upward sequence of clayey to sandy materials can be found on top, which indicates relatively a slight increase in fluvial energy during the deposition. It could have been formed synchronously with the underlying layer, since a similar thin layer of sandy material can be found within Fcb1 at KG07. All three locations are covered conformably by a colluvial layer with corresponding physical properties. The following sedimentary succession and units are positioned lower in the landscape (at roughly the same coordinates), therefore there must have been a period where the outflux of sediments was larger than the influx.

Only after this incision were the sediments of KG09 and XG02 deposited. Also at these locations the Ahmetler Formation is found. However, only about 2 m is exposed compared to the more than 6 m of the other locations. Various units unconformably overlie the Ahmetler Formation. In none of these units there is a clear flow direction visible. It may be the case that the flow was in the same orientation as the outcrop, as most units appear as semi-circular deposits, characteristic of the channel geometry. This would mean that the flow direction in these units was towards the SW and that all sediments came from the direction of the limestone plateau. The first unit that was deposited is Fcm1. As the name suggests, this unit contains metamorphic pebbles. Additionally, the carbonate pebbles are relatively small (~4 cm in diameter) and are mostly low-grade marbles. It is a thick unit (about 2 m) of cross-bedded sediments. The most likely source would be erosion from the basal conglomerates of the Ahmetler Formation which contain metamorphic fragments (Ersoy et al., 2010). This unit is unconformably overlain by units Fcb2 and Fc4. Fcb2, a unit consisting of large carbonate boulders (≤ 70 cm), is most likely the oldest unit of the two given its higher position in the outcrop. The other (presumably younger) units of this outcrop are all positioned lower and more to the east, disconnected from this unit. Therefore, it is highly unlikely that the stream deposited these sediments at a later stage at a higher elevation. The flow direction is along a NE-SW line, suggesting that the source material originated from the direction of the limestone plateau. Given the young age of the deposits, the basaltic pebbles in this unit were probably eroded from earlier deposits containing basaltic pebbles, possibly unit Fcb1. The large clasts and comparatively large surface area (~3 x 4 m) suggest a high energy environment with high erosion upstream. The following unit consists of only carbonate angular pebbles and boulders. It is deposited in a similar fashion as the sediments of unit Fc3, with the source being the limestone plateau. The lower position of this unit (and the following units) might be due to the presence of the fault in the layer underneath. The topographic imprint of this pre-Quaternary fault influenced the landscape and the fluvial regime. Slightly more to the east is the subsequent unit with a gradient of predominantly sand-sized material to a matrix with about 50 – 60% clasts. The clasts are of carbonate, basaltic and metamorphic origin suggesting a combination of erosion from the Ulubey and Ahmetler Formations and previously deposited sediments. This unit can also be found downstream at location XG02 and is conformably overlain by a thick layer only found at that location. The lack of this unit at KG09 indicates that it is either eroded or it was only deposited downstream, though it was impossible to determine. Still, the lower elevation of the subsequent unit Fcm2 at location KG09, suggests increased erosion. Although the lithology is the same as previous unit with carbonate and metamorphic pebbles, in this unit the layering is not as pronounced and the carbonate clasts are larger in size. However, the top half of this unit contains more low-grade marbles, whereas the bottom half more limestone clasts. This change in lithology is likely due to the incision into different units of Miocene/Quaternary deposits farther upstream. For the final two fluvial is was difficult to determine the order of deposition and might have been synchronous. However, the composition of both units is different, suggesting different sources.

Fcbm2 has more coarse material and contains pebbles of different lithologies. Fc6 consists predominantly of a sandy matrix with interfingering lenses of carbonate pebbles. The coarser sediments and clasts of Fcbm2 hint at more fluvial energy which could have partly eroded unit Fc6, However, this erosion is indistinguishable in the field. Overall, the change in lithological composition between the units does not seem to follow a clear trend and no exact source can be deduced. The presence of metamorphic pebbles only at location KG09 might suggest that, at that time incision was deep enough to reach the basal conglomerates of the Ahmetler Formation and prior to that it was not. Still, it seems that at times there is a shift in erosion from the Ulubey, Ahmetler Formations and/or more recent sediments causing an increase in carbonate, metamorphic and basaltic material, respectively.

5.2. OSL performance

Comparison of the quartz and feldspar ages reveals that the sediments are deposited not before ~2.5 ka. This age corresponds to the pottery pieces found in the same sedimentary succession, which were expected to be of Lydian or Hittite origin. These pieces must be older or of the same age than the deposits they were deposited in, which would put the burial age estimate at an age younger than ~3.7 ka (Garstang and Gurney, 1959). Sample NCL-1218132 seems to be of a younger age compared to the other samples (considering the 1σ uncertainties; Figure 21B). This is the case for both quartz and feldspar. Comparison between the ages of both minerals shows only disagreement with sample NCL-1218130. Cause for this discrepancy might be due to the quartz D_e distribution, which shows a very poorly bleached sample. Only about 6 aliquots fall within the MAM estimate, which also explains the relatively large error of that quartz age. Measuring additional aliquots increases the chance of observing more well bleached grains which in turn might lower the dose estimation, thus decreasing the estimated age. Overall, the quartz samples seem to have slightly older age estimates within a 67% confidence interval. Which might be due to the poor bleaching which in turn leads to averaging or because feldspar is in some way affected by anomalous fading. Since the fading test showed no clear signs of fading and because all samples show a poor D_e distribution, it is fair to assume that the overestimation of quartz is the most likely cause for the discrepancy between quartz and feldspar ages. Still, the ages do agree with each other within the 2σ uncertainty. Furthermore, within the 2σ errors, all the quartz ages are virtually indistinguishable. The feldspar ages, on the other hand, still indicate a significantly younger age for sample NCL-1218132.

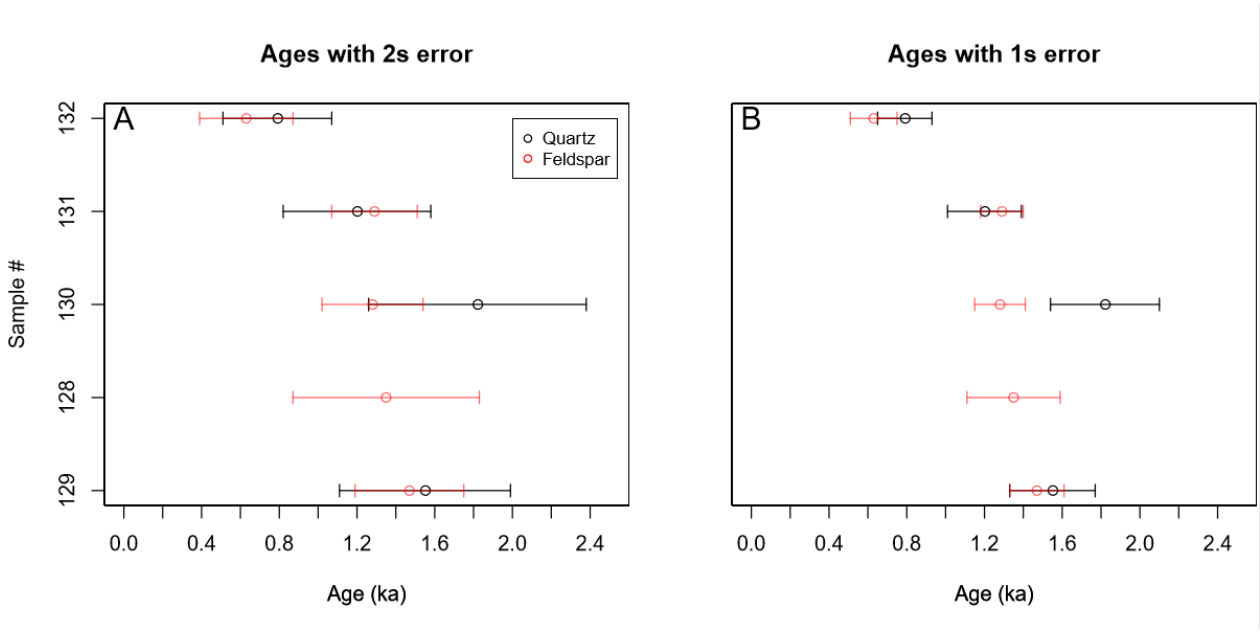

Figure 21 Quartz and feldspar ages all samples with the (A) 2 σ and (B) 1 σ uncertainty. The samples are shown in the stratigraphic order of their respective sedimentary unit.

Overall, the quartz and feldspar ages are in agreement within 2σ (Figure 21A). The fact that the OSL ages are internally consistent and in agreement with additional archaeological constraints supports the reliability of the datings. Also, the very small differences in ages indicate that the assumption of instant burial for the dose rate is adequate. However, as was made clear from the first quartz measurements it turned out that not every sampled sedimentary unit contained suitable quartz grains. This means that more samples are necessary to obtain the same amount of information as when using feldspar. More importantly, the quartz grains in this catchment produce a very weak signal. Because of this it takes more effort to obtain good signals, especially at a single grain level. This also means that multigrain aliquots are more unreliable since it is very likely that averaging occurs due to the lack of grains that give a strong signal. Feldspars do produce strong signals and with single grain measurements it was possible to extract the well bleached fraction. Furthermore, correlation with the stratigraphy shows that the feldspar ages are more in line with the stratigraphy compared to the more irregular ages of quartz. Additionally, with the applied protocol, there was limited to no influence of anomalous fading. Therefore, for this specific setting, OSL dating of feldspars is considered more reliable.

5.3. Context

The fact that sample NCL-1218132 somewhat differs in age compared to the other samples is consistent with the observations in the field. The sedimentary succession from which this sample was collected shows different characteristics and physical properties from other locations which lead to the conclusion of different time periods of deposition. This is further emphasised by the relative elevation of the units, which are about five metres lower in the landscape. Unfortunately, due to the lack of other samples in these units, the age cannot be verified with other ages. Though the consistency between quartz and feldspar ages is a good indicator in itself. Considering the feldspar ages, it can now be said that the time between the two distinguished successions is in the order of centuries/decades. The large differences in surface elevation of the badlands, the complex succession of the sedimentary units and the young ages all illustrate the dynamic nature of the badlands.

The very young age of the fluvial sediments means there is a gap in deposition between the Miocene sediments and late Holocene sediments. This implies that somewhere prior to the oldest Holocene deposition phase there must have been at least one period where incision was the most dominant process. Furthermore, the deposition of sediments around 1.3 ka (~700 A.D.) suggests more transportation of sediments around that time. The presence of multiple units containing boulder-sized clasts indicate high energy flow with which these boulders could be transported. An increase in fluvial activity, as a result of increased precipitation, would explain this succession. The ages of the deposits reveal that the deposition occurred during a time in which the conditions in the Mediterranean were wetter. Haldon et al. (2014) showed, by using a number of temperature and moisture proxies, that between 560 and 750 A.D. Anatolia experienced a wetter climate. Note that the studies used locations in Central Turkey and that this region has a different, more arid, climate due to presence of the Taurus mountains in the south (Beck et al., 2018) compared to Western Turkey. Still, it might have been part of a more (sub-)continental climatic trend which extends to Western Turkey. The increased deposition about 0.7 – 0.8 ka (~1300 A.D.) did not experience such a clear change in climate, though there have been reports of wetter conditions in the Mediterranean between the 11^{th} and 14^{th} century A.D. (Bakker et al., 2012). This climate influence could have been strengthened by a human response to the changing conditions, in which farmers would switch between agriculture and cattle grazing during wetter and dryer periods, respectively. This trend has been observed from pollen-records in SW Turkey (Bakker et al., 2012).

Unfortunately, the accuracy of the OSL measurements is insufficient to determine deposition rates as deposition and erosion in these badlands falls within the uncertainty of the ages. It is possible to distinguish different periods of dominant deposition, showing that there are (environmental) factors that govern the development of the badlands, which operate on larger time scales. At this stage it is still unclear what all these factors are and how much they contribute to the development of the badlands.

6. Conclusion

This study presents a stratigraphic reconstruction of the Kula Badlands, West Turkey, and demonstrates the implications for dating the sediments of this setting with OSL. Following a detailed reconstruction of the lithostratigraphy and depositional environments of a single sub-catchment within the badlands, the lithological differences and the properties of rocks have been established. The setting is characterised by a wide variety of mostly fluvial sediments ranging from fine-grained sand to boulder-sized clasts. A complex history of incision and aggradation can be observed. Certain locations were strategically selected for sample collection to test the feasibility of multi and single grain OSL dating techniques.

A multi-grain SAR protocol was applied to quartz grains and a single-grain regenerative pIRIR protocol to feldspar grains. By carrying out various performance tests the protocols could be tailored to these specific settings, which enabled us able to filter out the poorly bleached fraction. With both quartz and feldspar, it was possible to obtain realistic age estimations. Comparison of the estimated ages of both minerals have shown a reasonable agreement between three out of the four samples within a 95% confidence interval. A slight overestimation of the quartz ages is observed, which can be attributed to averaging of the signal. This averaging was a result of the low sensitivity of the grains which made it difficult to approach single grain measurements using multigrain aliquots. Furthermore, the feldspar pIRIR signal did not seem to be affected by anomalous fading and the ages were more in line with the stratigraphy. Therefore, the use of feldspar in dating the Kula Badlands sediments is considered to be more reliable. With the use of OSL two distinctive periods of aggradation have been dated, revealing ages of ~0.7 ka and 1.3 ka. The complexity of the sedimentary units, formed during this short amount of time, illustrates the highly dynamic nature of the badlands, which requires higher resolution data to be fully understood.

7. References

Aksay, S., 2018. Temperate Mediterranean Badlands: A (pre-)Holocene or Anthropocene phenomenon? PhD Research Proposal approved by PE & RC Graduate Research School of Wageningen University, (WU), the Netherlands. Project no. PE & RC 17063. https://www.wur.nl/en/show/TemperateMediterranean-Badlands-A-pre-Holocene-or-Anthropocene-phenomenon.htm.

Bakker, J., E. Paulissen, D. Kaniewski, V. De Laet, G. Verstraeten, and M. Waelkens. 2012. Man, vegetation and climate during the Holocene in the territory of Sagalassos, Western Taurus Mountains, SW Turkey. Veg. Hist. Archaeobot. 21(4): 249–266. doi: 10.1007/s00334-011-0312-4.

Beck, H.E., N.E. Zimmermann, T.R. McVicar, N. Vergopolan, A. Berg, and E.F. Wood. 2018. Present and future Köppen-Geiger climate classification maps at 1-km resolution. Sci. data 5: 180214.

Bøtter-Jensen, L., E. Bulur, G.A.T. Duller, and A.S. Murray. 2000. Advances in luminescence instrument systems. Radiat. Meas. 32(5): 523–528. doi: https://doi.org/10.1016/S1350-4487(00)00039-1.

Buylaert, J.-P., M. Jain, A.S. Murray, K.J. Thomsen, C. Thiel, and R. Sohbati. 2012. A robust feldspar luminescence dating method for Middle and Late Pleistocene sediments. Boreas 41(3): 435–451. doi: 10.1111/j.1502-3885.2012.00248.x.

Casana, J. 2008. Mediterranean valleys revisited: Linking soil erosion, land use and climate variability in the Northern Levant. Geomorphology 101(3): 429–442. doi: https://doi.org/10.1016/j.geomorph.2007.04.031.

Cerdà, A. 1999. Seasonal and spatial variations in infiltration rates in badland surfaces under Mediterranean climatic conditions. Water Resour. Res. 35(1): 319–328.

Clarke, M.L. 1996. IRSL dating of sands: Bleaching characteristics at deposition inferred from the use of single aliquots. Radiat. Meas. 26(4): 611–620. doi: https://doi.org/10.1016/1350-4487(96)00004-2.

Clarke, M.L., and H.M. Rendell. 2006. Process–form relationships in Southern Italian badlands: erosion rates and implications for landform evolution. Earth Surf. Process. Landforms J. Br. Geomorphol. Res. Gr. 31(1): 15–29.

Clarke, M.L., and H.M. Rendell. 2010. Climate-driven decrease in erosion in extant Mediterranean badlands. Earth Surf. Process. Landforms 35(11): 1281–1288.

Cunningham, A.C., and J. Wallinga. 2012. Realizing the potential of fluvial archives using robust OSL chronologies. Quat. Geochronol. 12: 98–106. doi: https://doi.org/10.1016/j.quageo.2012.05.007.

Cunningham, A.C., J. Wallinga, and P.S.J. Minderhoud. 2011. Expectations of scatter in equivalent-dose distributions when using multi-grain aliquots for OSL dating. Geochronometria 38(4): 424. doi: 10.2478/s13386-011-0048-z.

Duller, G.A.T. 2008. Single-grain optical dating of Quaternary sediments: why aliquot size matters in luminescence dating. Boreas 37(4): 589–612. https://onlinelibrary.wiley.com/doi/epdf/10.1111/j.1502-3885.2008.00051.x.

Duller, G. 2015. Riso Luminescence Analyst.

Duller, G.A.T., L. Bøtter-Jensen, and A.S. Murray. 2003. Combining infrared- and green-laser stimulation sources in single-grain luminescence measurements of feldspar and quartz. Radiat. Meas. 37(4):

543–550. doi: https://doi.org/10.1016/S1350-4487(03)00050-7.

Ercan, E., A. Türkecan, A. Dinçel, and A. Günay. 1983. Kula-Selendi (Manisa) dolaylarının jeolojisi [Geology of Kula-Selendi (Manisa) area]. Geol. Eng. 17: 3–28.

Ersoy, Y.E., C. Helvacı, and H. Sözbilir. 2010. Tectono-stratigraphic evolution of the NE–SW-trending superimposed Selendi basin: Implications for late Cenozoic crustal extension in Western Anatolia, Turkey. Tectonophysics 488(1–4): 210–232. doi: 10.1016/J.TECTO.2010.01.007.

Ersoy, Y., C. Helvacı, H. Sözbilir, F. Erkül, and E. Bozkurt. 2008. A geochemical approach to Neogene–Quaternary volcanic activity of western Anatolia: An example of episodic bimodal volcanism within the Selendi Basin, Turkey. Chem. Geol. 255(1): 265–282. doi: https://doi.org/10.1016/j.chemgeo.2008.06.044.

Faulkner, H., D. Spivey, and R. Alexander. 2000. The role of some site geochemical processes in the development and stabilisation of three badland sites in Almerıa, Southern Spain. Geomorphology 35(1–2): 87–99.

G. Wintle, A., S. Li, G. Botha, and J. C. Vogel. 1995. Evaluation of luminescence-dating procedures applied to late- Holocene colluvium near St Paul's Mission, Natal, South Africa.

Galbraith, R.F., R.G. Roberts, G.M. Laslett, H. Yoshida, and J.M. Olley. 1999. Optical dating of single and multiple grains of quartz from Jinmium rock shelter, northern Australia: Part I, experimental design and statistical models. Archaeometry 41(2): 339–364.

García-Ruiz, J.M., E. Nadal-Romero, N. Lana-Renault, and S. Beguería. 2013. Erosion in Mediterranean landscapes: changes and future challenges. Geomorphology 198: 20–36.

Garstang, J., and O.R. Gurney. 1959. The geography of the Hittite empire. British Institute of Archaeology at Ankara.

Godfrey-Smith, D.I., D.J. Huntley, and W.-H. Chen. 1988. Optical dating studies of quartz and feldspar sediment extracts. Quat. Sci. Rev. 7(3): 373–380. doi: https://doi.org/10.1016/0277-3791(88)90032-7.

Van Gorp, W., J.M. Schoorl, A.J.A.M. Temme, T. Reimann, J.R. Wijbrans, D. Maddy, T. Demir, and T. Veldkamp. 2016. Catchment response to lava damming: integrating field observation, geochronology and landscape evolution modelling. Earth Surf. Process. Landforms 41(11): 1629–1644. doi: 10.1002/esp.3981.

Van Gorp, W., A.J.A.M. Temme, J.E.M. Baartman, and J.M. Schoorl. 2014. Landscape Evolution Modelling of naturally dammed rivers. Earth Surf. Process. Landforms 39(12): 1587–1600. doi: 10.1002/esp.3547.

Van Gorp, W., A. Veldkamp, A.J.A.M. Temme, D. Maddy, T. Demir, T. van der Schriek, T. Reimann, J. Wallinga, J. Wijbrans, and J.M. Schoorl. 2013. Fluvial response to Holocene volcanic damming and breaching in the Gediz and Geren rivers, western Turkey. Geomorphology 201: 430–448. doi: 10.1016/J.GEOMORPH.2013.07.016.

Haldon, J., N. Roberts, A. Izdebski, D. Fleitmann, M. McCormick, M. Cassis, O. Doonan, W. Eastwood, H. Elton, S. Ladstätter, S. Manning, J. Newhard, K. Nicoll, I. Telelis, and E. Xoplaki. 2014. The Climate and Environment of Byzantine Anatolia: Integrating Science, History, and Archaeology. J. Interdiscip. Hist. 45(2): 113–161. doi: 10.1162/JINH_a_00682.

Jain, M., and C. Ankjærgaard. 2011. Towards a non-fading signal in feldspar: Insight into charge transport and tunnelling from time-resolved optically stimulated luminescence. Radiat. Meas. 46(3): 292–309. doi: https://doi.org/10.1016/j.radmeas.2010.12.004.

Kars, R.H., T. Reimann, C. Ankjærgaard, and J. Wallinga. 2014. Bleaching of the post-IR IRSL signal: new insights for feldspar luminescence dating. Boreas 43(4): 780–791. doi: 10.1111/bor.12082.

Kreutzer, S., C. Burow, M. Dietze, M.C. Fuchs, C. Schmidt, M. Fischer, and J. Friedrich. 2018. Luminescence: Comprehensive Luminescence Dating Data Analysis. https://cran.r-project.org/package=Luminescence.

Kuhn, N.J., A. Yair, and M.K. Grubin. 2004. Spatial distribution of surface properties, runoff generation and landscape development in the Zin Valley Badlands, northern Negev, Israel. Earth Surf. Process. Landforms J. Br. Geomorphol. Res. Gr. 29(11): 1417–1430.

Lian, O.B., J. Hu, D.J. Huntley, and S.R. Hicock. 1995. Optical dating studies of Quaternary organic-rich sediments from southwestern British Columbia and northwestern Washington State. Can. J. Earth Sci. 32(8): 1194–1207.

Lukas, S., J.Q.G. Spencer, R.A.J. Robinson, and D.I. Benn. 2007. Problems associated with luminescence dating of Late Quaternary glacial sediments in the NW Scottish Highlands. Quat. Geochronol. 2(1): 243–248. doi: https://doi.org/10.1016/j.quageo.2006.04.007.

Maddy, D., T. Demir, D.R. Bridgland, A. Veldkamp, C. Stemerdink, T. van der Schriek, and R. Westaway. 2008. The Early Pleistocene development of the Gediz River, Western Turkey: An uplift-driven, climate-controlled system? Quat. Int. 189(1): 115–128. doi: 10.1016/J.QUAINT.2007.08.045.

Maddy, D., D. Schreve, T. Demir, A. Veldkamp, J.R. Wijbrans, W. van Gorp, D.J.J. van Hinsbergen, M.J. Dekkers, R. Scaife, J.M. Schoorl, C. Stemerdink, and T. van der Schriek. 2015. The earliest securely-dated hominin artefact in Anatolia? Quat. Sci. Rev. 109: 68–75. doi: https://doi.org/10.1016/j.quascirev.2014.11.021.

Murray, A.S., and A.G. Wintle. 2000. Luminescence dating of quartz using an improved single-aliquot regenerative-dose protocol. Radiat. Meas. 32(1): 57–73. doi: https://doi.org/10.1016/S1350-4487(99)00253-X.

Murray, A.S., and A.G. Wintle. 2003. The single aliquot regenerative dose protocol: potential for improvements in reliability. Radiat. Meas. 37(4): 377–381. doi: https://doi.org/10.1016/S1350-4487(03)00053-2.

Nadal-Romero, E., J.F. Martínez-Murillo, M. Vanmaercke, and J. Poesen. 2011. Scale-dependency of sediment yield from badland areas in Mediterranean environments. Prog. Phys. Geogr. 35(3): 297–332.

Pietsch, T.J., J.M. Olley, and G.C. Nanson. 2008. Fluvial transport as a natural luminescence sensitiser of quartz. Quat. Geochronol. 3(4): 365–376. doi: https://doi.org/10.1016/j.quageo.2007.12.005.

Preusser, F., K. Ramseyer, and C. Schlüchter. 2006. Characterisation of low OSL intensity quartz from the New Zealand Alps. Radiat. Meas. 41(7): 871–877. doi: https://doi.org/10.1016/j.radmeas.2006.04.019.

Purvis, M., and A. Robertson. 2004. A pulsed extension model for the Neogene–Recent E–W-trending Alaşehir Graben and the NE–SW-trending Selendi and Gördes Basins, western Turkey.

Tectonophysics 391(1): 171–201. doi: https://doi.org/10.1016/j.tecto.2004.07.011.

Reimann, T., S. Lindhorst, K.J. Thomsen, A.S. Murray, and M. Frechen. 2012a. OSL dating of mixed coastal sediment (Sylt, German Bight, North Sea). Quat. Geochronol. 11: 52–67. doi: https://doi.org/10.1016/j.quageo.2012.04.006.

Reimann, T., K.J. Thomsen, M. Jain, A.S. Murray, and M. Frechen. 2012b. Single-grain dating of young sediments using the pIRIR signal from feldspar. Quat. Geochronol. 11: 28–41. doi: 10.1016/J.QUAGEO.2012.04.016.

Reimann, T., and S. Tsukamoto. 2012. Dating the recent past (<500 years) by post-IR IRSL feldspar – Examples from the North Sea and Baltic Sea coast. Quat. Geochronol. 10: 180–187. doi: https://doi.org/10.1016/j.quageo.2012.04.011.

Reimann, T., S. Tsukamoto, M. Naumann, and M. Frechen. 2011. The potential of using K-rich feldspars for optical dating of young coastal sediments – A test case from Darss-Zingst peninsula (southern Baltic Sea coast). Quat. Geochronol. 6(2): 207–222. doi: https://doi.org/10.1016/j.quageo.2010.10.001.

Rhodes, E.J. 2011. Optically Stimulated Luminescence Dating of Sediments over the Past 200,000 Years. Annu. Rev. Earth Planet. Sci. 39(1): 461–488. doi: 10.1146/annurev-earth-040610-133425.

Richardson-Bunbury, J.M. 1996. The Kula Volcanic Field, western Turkey: the development of a Holocene alkali basalt province and the adjacent normal-faulting graben. Geol. Mag. 133(3): 275–283. doi: DOI: 10.1017/S0016756800009018.

Seyitoğlu, G. 1997. Late Cenozoic tectono-sedimentary development of the Selendi and Uşak-Güre basins: a contribution to the discussion on the development of east–west and north trending basins in western Turkey. Geol. Mag. 134(2): 163–175. doi: DOI: undefined.

Smedley, R.K., G.A.T. Duller, N.J.G. Pearce, and H.M. Roberts. 2012. Determining the K-content of single-grains of feldspar for luminescence dating. Radiat. Meas. 47(9): 790–796. doi: https://doi.org/10.1016/j.radmeas.2012.01.014.

Smedley, R.K., G.A.T. Duller, and H.M. Roberts. 2015. Bleaching of the post-IR IRSL signal from individual grains of K-feldspar: Implications for single-grain dating. Radiat. Meas. 79: 33–42. doi: https://doi.org/10.1016/j.radmeas.2015.06.003.

Steffen, D., F. Preusser, and F. Schlunegger. 2009. OSL quartz age underestimation due to unstable signal components. Quat. Geochronol. 4(5): 353–362. doi: https://doi.org/10.1016/j.quageo.2009.05.015.

Thomsen, K.J., A.S. Murray, M. Jain, and L. Bøtter-Jensen. 2008. Laboratory fading rates of various luminescence signals from feldspar-rich sediment extracts. Radiat. Meas. 43(9): 1474–1486. doi: https://doi.org/10.1016/j.radmeas.2008.06.002.

Vasiliniuc, Ş., D.A.G. Vandenberghe, A. Timar-Gabor, C. Cosma, and P. van den Haute. 2013. Combined IRSL and post-IR OSL dating of Romanian loess using single aliquots of polymineral fine grains. Quat. Int. 293: 15–21. doi: https://doi.org/10.1016/j.quaint.2012.01.002.

Veldkamp, A., I. Candy, A.G. Jongmans, D. Maddy, T. Demir, J.M. Schoorl, D. Schreve, C. Stemerdink, and T. van der Schriek. 2015. Reconstructing Early Pleistocene (1.3 Ma) terrestrial environmental change in western Anatolia: Did it drive fluvial terrace formation? Palaeogeogr. Palaeoclimatol. Palaeoecol. 417: 91–104. doi: 10.1016/J.PALAEO.2014.10.022.

Wallinga, J. 2008. Optically stimulated luminescence dating of fluvial deposits: a review. Boreas 31(4): 303–322. doi: 10.1111/j.1502-3885.2002.tb01076.x.

Wallinga, J., A.J.J. Bos, P. Dorenbos, A.S. Murray, and J. Schokker. 2007. A test case for anomalous fading correction in IRSL dating. Quat. Geochronol. 2(1): 216–221. doi: https://doi.org/10.1016/j.quageo.2006.05.014.

Wallinga, J., A. Murray, and A. Wintle. 2000. The single-aliquot regenerative-dose (SAR) protocol applied to coarse-grain feldspar. Radiat. Meas. 32(5): 529–533. doi: https://doi.org/10.1016/S1350-4487(00)00091-3.

Wintle, A.G., S.H. Li, G.A. Botha, and J.C. Vogel. 1995. Evaluation of luminescence-dating procedures applied to late-Holocene colluvium near St Paul's Mission, Natal, South Africa. The Holocene 5(1): 97–102. doi: 10.1177/095968369500500110.

Wintle, A.G., and A.S. Murray. 2006. A review of quartz optically stimulated luminescence characteristics and their relevance in single-aliquot regeneration dating protocols. Radiat. Meas. 41(4): 369–391. doi: https://doi.org/10.1016/j.radmeas.2005.11.001.

8. Appendix

Table A Quartz SAR protocol for the dose recovery and equivalent dose measurements.

Step	Settings	D_e	DR
Bleaching	2x Blue LED OSL; 30 °C, 300 s	No	Yes
First irradiation	Beta irradiation	Empty	4.1
Irradiation (regenerative)	Beta irradiation (Gy)	4.1, 8.2, 16.4, 41.0, 123.2, 0, 4.1, 4.1(IR)	4.9, 9.8, 0, 4.9, 4.9(IR)
Preheat	200 °C, 10 s	Yes	Yes
IR-scan (final run)	(IR LED OSL; 30 °C, 40 s)	Yes	Yes
Measurement	Blue LED OSL; 125 °C, 20 s	Yes	Yes
Test dose irradiation	Beta irradiation; ~4.1 Gy	Yes	Yes
Cut heat	180 °C, 10 s	Yes	Yes
Test dose measurement	Blue LED OSL; 125 °C, 20 s	Yes	Yes
Clean signal	Blue LED OSL; 210 °C, 40 s	Yes	Yes

Table B Quartz SAR protocol for the thermal transfer and preheat plateau tests.

Step	Settings	TT	Php + DR
Bleaching	2x Blue LED OSL; 30 °C, 300 s	Yes	Yes
First irradiation	Beta irradiation (Gy)	Empty	6.2
Irradiation (regenerative)	Beta irradiation (Gy)	4.1, 0, 4.1, 4.1(IR)	6.2, 4.1, 8.2, 16.4, 0, 4.1, 4.1(IR)
Preheat	180 -280 °C, 10 s	Yes	Yes
IR-scan	(IR LED OSL; 30 °C, 40 s)	Yes	Yes
Measurement	Blue LED OSL; 125 °C, 20 s	Yes	Yes
Test dose irradiation	Beta irradiation; ~4.1 Gy	Yes	Yes
Cut heat	160 - 220 °C, 10 s	Yes	Yes
Test dose measurement	Blue LED OSL; 125 °C, 20 s	Yes	Yes
Clean signal	Blue LED OSL; 190 - 290 °C, 40 s	Yes	Yes

Table C Quartz single grain regenerative protocol for the determination of equivalent doses.

Step	Settings
Irradiation (Gy) (regenerative)	Beta: Nat, 5, 10, 20, 50, 100, 0, 50, 50
Preheat	200 °C, 10 s
IR-scan (final run)	IR LED OSL; 30 °C, 40 s
Measurement	SG green laser; 125 °C, 1 s
Test dose irradiation	Beta irradiation; 5 Gy
Cut heat	180 °C, 10 s
Test dose measurement	SG green laser; 125 °C, 1 s
Clean signal	Blue LED OSL; 210 °C, 40 s

Table D Feldspar Single grain pIRIR sequence for the measurements of the dose recovery test, the residual signal and the equivalent doses.

Step	Settings	D_e	DR	Residual
Bleaching	Solar simulator; 2 d	No	Yes	Yes
First irradiation	Beta irradiation (Gy)	Empty (natural)	10	Empty
Irradiation (regenerative)	Beta irradiation (Gy)	5, 10, 20, 40, 80, 160, 0, 10	7.5, 15, 30, 60, 0, 15	7.5, 15, 0, 15
Preheat	200 °C, 60 s	Yes	Yes	Yes
Measurement	SG IR laser; 50 °C, 2 s	Yes	Yes	Yes
Measurement pIRIR	SG IR laser; 175 °C, 2 s	Yes	Yes	Yes
Clean signal	IR LED OSL; 175 °C, 500 s	Yes	Yes	Yes
Test dose irradiation	Beta irradiation; 10 Gy	Yes	Yes	Yes
Preheat	200 °C, 60 s	Yes	Yes	Yes
Test dose measurement	SG IR laser; 50 °C, 2 s	Yes	Yes	Yes
Test dose measurement pIRIR	SG IR laser; 175 °C, 2 s	Yes	Yes	Yes
Clean signal	IR LED OSL; 175 °C, 500 s	Yes	Yes	Yes

Table E Set-up of the anomalous fading sequence where for each disc the total time in seconds is calculated. For every step the time it takes to perform that step is shown.

Step	Run 1	Run 2	Run 3	Run 4	Run 5	Run 6	Run 7	Run 8	Run 9	Run 10	Run 11	Run 12	Run 13	Run 14
Total pause time	Irradiation	Pre-heat	Pause	IR50(SG)	IR175(SG)	bleaching	Td irradiat	cut-heat	IR50(SG)	IR175(SG)	bleaching	Irradiation	preheat	pause
150	100	100		210	235	535	50	100	210	235	535	100	110	
10240				210	235	535	50	100	210	235	535			410
150	100	100		210	235	535	50	100	210	235	535	100	110	
	Pauze	180000												
190240				210	235	535	50	100	210	235	535			410
1000	100	100	850	210	235	535	50	100	210	235	535			
150	100	100		210	235	535	50	100	210	235	535	100	110	
10240				210	235	535	50	100	210	235	535			410
1000	100	100	850	210	235	535	50	100	210	235	535			